

THE LIFT OF THIN AIRFOILS AT HIGH-SUBSONIC SPEEDS

Thesis by
William W. Willmarth

In Partial Fulfillment of the Requirements
For the Degree of
Doctor of Philosophy

California Institute of Technology
Pasadena, California

1954

ACKNOWLEDGMENTS

The assistance and encouragement of Dr. H. W. Liepmann and Dr. J. D. Cole throughout the course of the present research program is gratefully acknowledged. The author is indebted to Mr. R. Hakkinen, Dr. G. Solomon and Mr. K. Krishnamurty for their help with the experiments and to Mrs. J. Cottingham and Miss C. Baum who prepared the report and figures for publication.

ABSTRACT

Experimental results are presented for the lift characteristics of thin, two-dimensional airfoils at high-subsonic speeds and small angles of attack. Symmetrical airfoils with different locations of maximum thickness were investigated using a surface pressure probe technique which should find use in other applications.

The flow fields over each airfoil are discussed and the quantitative results for the lift and location of the center of lift are compared with theory whenever possible. The effects of flow separation caused by boundary-layer shock-wave interaction are noted and discussed. In particular, the possibility of the forced oscillation of control surfaces due to boundary layer separation is mentioned.

TABLE OF CONTENTS

Acknowledgments	i
Abstract	ii
Table of Contents	iii
Symbols	iv
I. Introduction	1
II. A Qualitative Description of the Flow Over a Lifting Profile at Transonic Speeds	5
1. Zero Angle of Attack	5
2. Small Angle of Attack	8
3. Larger Angles of Attack	10
III. Description of Airfoils and Experimental Techniques	15
1. Description of Airfoils	15
2. Experimental Technique and Apparatus	16
IV. Experimental Results	21
1. Truncated Wedge	22
2. Round Nose Airfoil	27
3. Double Wedges, $t/c = 0.053$ and 0.104	30
4. Summary of Lift and Drag Results	38
V. Conclusions	41
Appendices	
A. Airfoil Characteristics Near Mach Number One	43
B. The Measurement of Surface Pressure with Static Probes	47
C. Computation of the Lift of a Truncated Wedge	50
References	61
Figures	64

SYMBOLS

a sound velocity

c airfoil chord

C_D pressure drag coefficient per unit span

\tilde{C}_D reduced drag coefficient, $C_D \frac{(\gamma+1)^{1/3}}{(t/c)^{5/3}} = \tilde{C}_D$

C_L lift coefficient per unit span

\tilde{C}_L reduced lift coefficient, $C_L [(\gamma+1) t/c]^{1/3}$ or $C_L [(\gamma+1) \delta]^{1/3} = \tilde{C}_L$

C_m moment coefficient about leading edge per unit length

C_p pressure coefficient

M Mach number based on local speed of sound

M^* Mach number based on speed of sound at sonic velocity

p pressure

q dynamic pressure

t/c airfoil thickness ratio

U free stream velocity

u horizontal component perturbation velocity

v vertical component perturbation velocity

x, y Cartesian coordinates, origin at leading edge of profile

α angle of attack

γ ratio of specific heats (1.4 for air)

δ wedge nose semi-angle

ξ reduced Mach number, $\frac{1-M^2}{[(\gamma+1) t/c]^{2/3}}$ or $\frac{1-M^2}{[(\gamma+1) \delta]^{2/3}} = \xi$

Subscripts and Superscripts

$()_{\infty}$ conditions in free stream

$()^*$ conditions at sonic velocity, note that M^* is not included

symbols used without subscripts indicate local conditions

I. INTRODUCTION

When a body moves through a compressible fluid at constant low subsonic or high supersonic speeds the fluid velocity relative to the body remains, in most cases, entirely subsonic or entirely supersonic. At transonic speeds, between the above extremes, the fluid velocity will be both subsonic and supersonic in the flow field near the body. The complicated mixed subsonic and supersonic flow patterns, which occur at transonic speeds, have been the subject of many experimental and theoretical investigations.

Much of the experimental work already published on steady transonic flow has been concerned with lifting two-dimensional profiles. However, most of this work has dealt with specific profiles or was done for a specific purpose with direct application to immediate design problems. Accordingly, the present investigation was initiated with the purpose of systematically investigating and describing the steady, two-dimensional flow over thin, lifting airfoils at transonic speeds and small angles of attack. The experiments should help in understanding the qualitative behavior of wing and control surfaces at transonic speeds.

The present investigation of lifting profiles was also a natural extension of previous experimental work done at GALCIT by Bryson and Solomon. Bryson (Ref. 1) examined the transonic flow at zero angle of attack over two-dimensional wedge and circular arc forebodies followed by a straight afterbody. Solomon (Ref. 2) considered axially-symmetric transonic flow over cone cylinder sections. The above investigations of flow over forebodies were not unduly complicated by viscous

effects. The surface pressure gradients ahead of the point of maximum thickness were favorable, thus minimizing boundary layer growth. In addition, the shock waves, which occurred at subsonic speeds, intersected the body surface downstream of the point of maximum thickness, where their effect on the forebody was small.

Lifting two-dimensional profiles present a more complicated problem than the above forebody investigations, since closed profiles, made up of a forebody and an afterbody, must be considered. The adverse pressure gradients over the afterbody cause the boundary layer to grow rapidly and make separation possible. In addition, shock waves are usually present on the afterbody surface at subsonic speeds. The shock waves often cause boundary layer separation with subsequent loss of lift. The realization of the importance of boundary-layer shock-wave interaction for lifting bodies is not new (Ref. 3), but can hardly be over-emphasized.

In spite of the importance of viscous effects, a great deal of information about lifting two-dimensional profiles has already been obtained from theoretical work with the non-viscous transonic equations of motion (Ref. 4). In particular, von Kármán (Ref. 4) and Busemann (Ref. 5), followed by Spreiter (Ref. 6) and Harder (Ref. 7) have discussed various forms of similarity laws based on the transonic equations. In addition, Guderley and Yoshihara (Ref. 8) have obtained a solution in the hodograph plane, where the transonic equations are linear, for the lift of a double wedge with small angle of attack at a free stream Mach number of one. Between Mach number one and the attachment Mach numbers Vincenti and Wagoner (Ref. 9) have done a relaxation computation

in the hodograph plane for the lift of a double wedge at small angles of attack.

At subsonic speeds there are, of course, many solutions based upon the Prandtl-Glauert similarity law and well known incompressible flow solutions. However, when shock waves appear in the flow field the Prandtl-Glauert similarity law breaks down. Recently Gullstrand (Ref. 10) obtained an approximate solution, in the physical plane, for the lift of a 6 percent thick symmetrical parabolic arc profile at small angles of attack with shock waves present on the airfoil surface. Gullstrand's results showed that as the Mach number increased, the lift curve slope rose to values above those given by the Prandtl-Glauert law and then fell rapidly only to rise again to a constant value at speeds near Mach number one.

Another result, which is very useful, is the principle of stationarity for flows near Mach number one. The stationarity of a flow near Mach number one was discussed by Liepmann and Bryson (Ref. 11). They based their discussion on the well-known result that the Mach number behind a normal shock wave is approximately $1 - \epsilon$ when the Mach number ahead of the shock is $1 + \epsilon$, where $\epsilon \ll 1$. At supersonic speeds with Mach number equal to $1 + \epsilon$ the detached bow wave is far upstream, so that the body, in effect, is immersed in an approximately uniform subsonic flow at Mach number $1 - \epsilon$. Therefore, as $\epsilon \rightarrow 0$ the local Mach number near the body does not change, which is expressed by the condition $\partial M / \partial M_\infty = 0$ near $M_\infty = 1$. This principle is used in Appendix A to derive an expression for the lift coefficient at Mach number one.

As mentioned previously, a great deal of experimental work has been done on lifting two-dimensional profiles at transonic speeds. In the discussion of the present experiments, mention will be made of previous work where it applies.

In order to obtain a better understanding of the flow patterns for lifting profiles, the next section gives a qualitative description of steady flow over a two-dimensional profile at transonic speeds.

II. A QUALITATIVE DESCRIPTION OF THE FLOW OVER A LIFTING PROFILE AT TRANSONIC SPEEDS

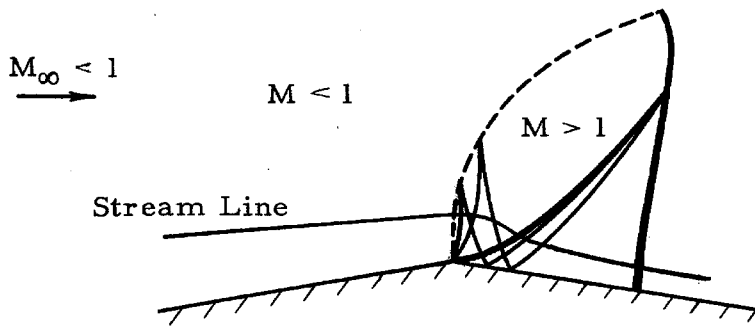
In order to discuss the main features of steady, two-dimensional, transonic flow patterns, the relatively simple lifting double wedge will be considered. The flow at zero angle of attack is well known (Refs. 12, 13, and 14), however, a brief review will be given. Next, the changes to be expected when the wedge is at small angle of attack will be discussed.

1. Zero Angle of Attack

From the experimental work of Bryson (Ref. 1) and Griffith (Ref. 15), it is apparent that the flow patterns over a given body change smoothly and continuously with free stream Mach number. This principle gives a valuable check on the accuracy of the following discussion.

At zero angle of attack and low subsonic speeds, the flow of air over a thin double wedge is everywhere subsonic. The velocity is a maximum at the sharp corner formed by the intersection of the wedge flanks. A non-viscous compressible fluid would, however, attain at least sonic velocity at the corner. This is not the case for a viscous fluid flowing at low subsonic speeds, since the boundary layer "rounds off" the corner.

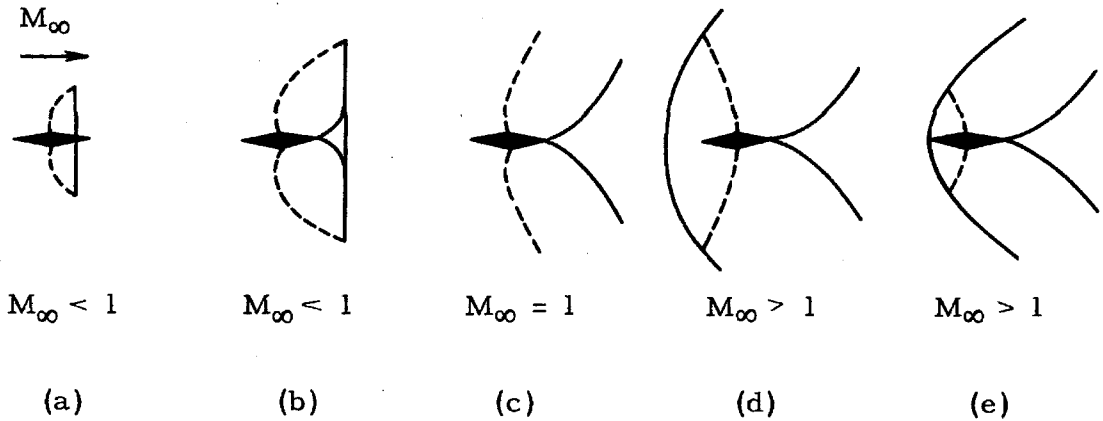
At higher subsonic speeds the air velocity, in the vicinity of the wedge shoulder, does not remain subsonic in spite of the effect of the boundary layer. Sketch 1 shows a half wedge at a subsonic free stream Mach number, such that the air velocity is supersonic near the wedge



Sketch 1

shoulder. The local supersonic region is bounded by a sonic line (dashed), the body surface, and a terminating shock wave which is approximately normal. At the corner, the sonic line is normal to the front flank of the wedge. The flow very near the corner is locally Prandtl-Meyer with expansion characteristics running from the corner to the sonic line, where they are reflected as compression characteristics which intersect the body surface. Guderley (Ref. 12) has shown that upon reflection from the body surface, the compression characteristics coalesce to form a weak oblique shock wave running from just behind the corner out into the supersonic region. This oblique shock, a few characteristics, and a typical streamline are shown in Sketch 1, but will be omitted from the succeeding discussion.

Sketch 2a shows the complete wedge at zero angle of attack and the above low subsonic Mach number. In Sketch 2b the Mach number is higher but still subsonic. The original supersonic region now covers the entire afterbody. Oblique shocks now arise at the trailing edge and deflect the flow over the wedge afterbody to a direction approximately parallel to the free stream direction. They leave the air velocity



Sketch 2

supersonic, so that an approximately normal shock behind the double wedge is necessary to terminate the supersonic region.

As M_∞ approaches one, the flow over the wedge remains essentially the same. The supersonic zone, however, becomes larger until at $M_\infty = 1$ (Sketch 2c), the terminating normal shock has receded infinitely far downstream and the sonic lines from the wedge shoulder extend to infinity above and below the body.

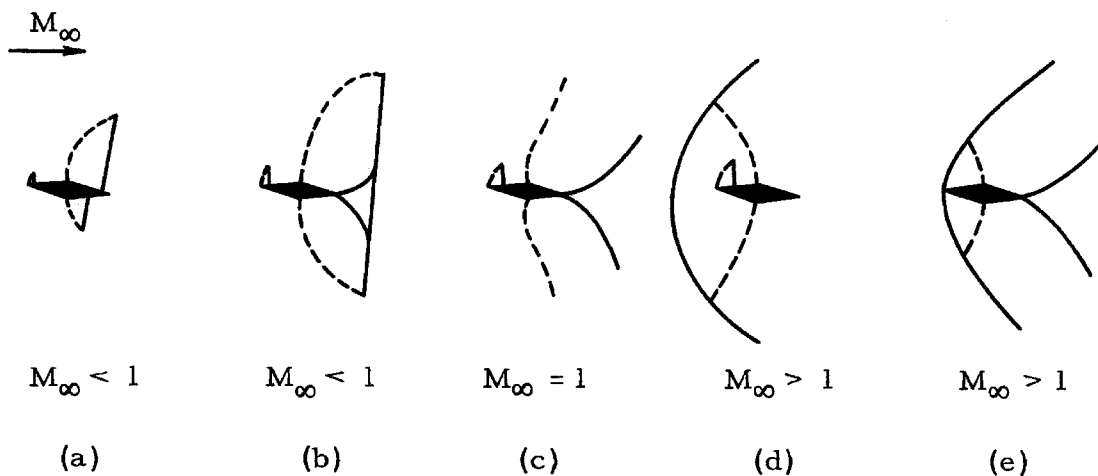
Since the sonic lines, at $M_\infty = 1$, extend to infinity above and below the airfoil, the rear portion of the body should have no effect on the front portion. The exact line of separation between the front and rear flow fields is not the sonic line but the limiting Mach line as discussed by Guderley and Yoshihara (Ref. 13). The limiting Mach line, in the present case, is the last expansion characteristic from the wedge shoulder, which intersects the sonic line at infinity. Since there are expansion characteristics both upstream and downstream of the limiting Mach line, only that portion of the shoulder expansion which is

upstream of the limiting Mach line can influence the subsonic flow over the wedge forebody. The fore- and afterbody flow fields for $M_\infty \geq 1$ are thus separated.

At higher supersonic speeds (Sketch 2d) a curved bow wave appears far ahead of the body. The sonic lines now run from the wedge shoulder to the shock. The subsonic zone ahead of the body is bounded by the bow shock, the wedge forebody, and sonic lines. At still higher supersonic speeds (sketch 2e), the curved bow wave attaches and further reduces the size of the subsonic zone. At still higher speeds the bow shock is straight and the flow over the forebody becomes uniform with a Mach number equal to or greater than one.

2. Small Angle of Attack

The change in the above symmetrical flow patterns due to a small angle of attack can now be discussed. Briefly, the shock wave positions at low subsonic speeds (Sketch 3a) are not symmetrical, because the air



Sketch 3

flowing over the upper surface is expanded more than that flowing over the lower surface. Thus, the upper supersonic zone becomes larger than the lower one. In addition, a small supersonic zone arises due to the expansion of the air flowing around the nose. This small supersonic zone is again bounded by a sonic line, a terminating shock, and the body surface near the nose.

The velocity at any given point on the lower surface of the double wedge is now less than that at a corresponding point on the upper surface. Thus, a pressure difference exists which can be integrated to give the lift and moment acting on the airfoil. At higher subsonic speeds (Sketch 3b), the main supersonic zone now encloses the entire rear half of the airfoil, and the terminating normal shocks are no longer on the body (the small nose supersonic zone also grows slightly larger). The Kutta condition is now satisfied locally by unsymmetrical shock waves at the trailing edge through which the flow from the upper and lower surfaces is deflected to give an approximately parallel stream with a small amount of downwash. At Mach number one (Sketch 3c), the nose supersonic zone is again larger, but the over-all flow pattern near the body is unchanged. The terminating shock has receded infinitely far downstream. At higher supersonic speeds (Sketch 3d) an unsymmetrical, curved bow wave appears ahead of the body, while the nose supersonic region again grows larger. The main supersonic zone over the upper half of the afterbody remains larger than that over the lower half. Thus, the subsonic zone ahead of the wedge forebody is larger on the bottom half than on the top. The portion of the bow shock which is normal to the free stream will now be slightly below the position it occupied at

zero angle of attack. With a further increase in Mach number, the bow shock attaches and isolates the upper and lower surface flow fields (Sketch 3e) causing the disappearance of the supersonic zone at the nose. The bow shock will be curved on the lower side with subsonic flow behind the shock. On the top side the flow may be subsonic with a curved shock or supersonic with a straight shock. The type of flow on the upper side depends on the Mach number, angle of attack, and wedge included angle. It is shown as subsonic on both sides in Sketch 3e. Finally, at higher Mach numbers the attached shocks both become straight and the velocity is everywhere supersonic.


From the above discussion, the main features concerning the growth of the supersonic regions have been considered. Similar flow patterns have been observed on curved symmetrical airfoils when the angle of attack is small, although the location of the sonic line on a curved surface changes somewhat with free stream Mach number, except at $M_{\infty} = 1$.

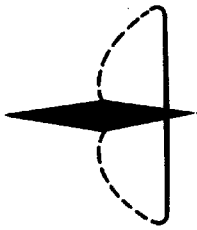
For symmetrical airfoils at small angles of attack, Spreiter (Ref. 6) has suggested that the pressure increment due to angle of attack should change linearly with α , if $\alpha \ll t/c$, so that C_L would be proportional to α . This assumption was checked experimentally and is discussed in Section IV. Also, the effects of boundary layer growth and possible separation have not been mentioned but are considered later where they arise in the experimental results.

3. Larger Angles of Attack

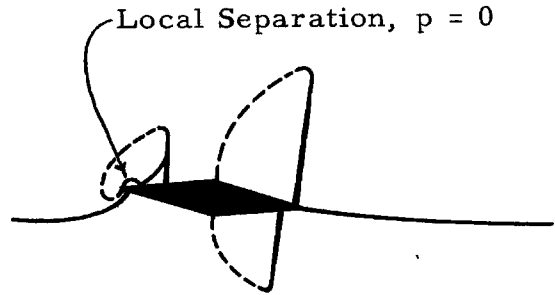
It is also interesting to consider the changes in the flow field

about a double wedge when only the angle of attack is varied. For this purpose, the free stream Mach number is assumed to be subsonic, yet high enough to give supersonic zones behind the wedge shoulder. As before, the supersonic zones are terminated by shocks on the airfoil (Sketch 4a).

$M_\infty < 1$


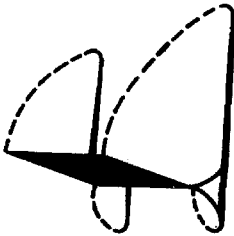


(a) $\alpha = \alpha_a = 0$

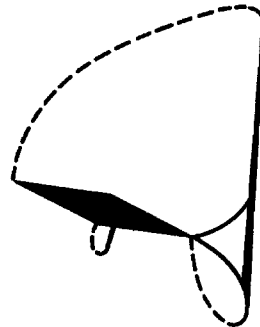


Zero Stream Line

(b) $\alpha_b > \alpha_a$



(c) $\alpha_c > \alpha_b$



(d) $\alpha_d > \alpha_c$

Sketch 4

When the angle of attack is increased to a small angle the flow pattern (Sketch 4b) is the same as that of Sketch 3a. A consideration

of the non-viscous flow over the wedge nose leads to the conclusion that the flow must separate locally on the upper surface near the nose.

The flow over the wedge nose has been discussed by Guderley and Yoshihara (Ref. 8). They considered the flow in the physical and hodograph planes. From their discussion it is apparent that the zero streamline branches at the stagnation point just under the nose of the wedge. From the stagnation point, the upper branch of the zero streamline flows forward along the lower surface of the wedge until sonic velocity is attained at the nose. The flow then turns through a large angle in going around the sharp nose. The turning is accomplished by a local, Prandtl-Meyer expansion. For thin wedges the expansion required can easily exceed the maximum turning angle (approximately 135°) for a Prandtl-Meyer expansion. Hence, the flow must separate locally at the nose. After the local separation, the flow is turned back toward the upper surface of the wedge, because the static pressure increases as one moves upward and away from the wedge surface. At the point of flow reattachment, an oblique shock appears which readjusts the flow direction so that the zero streamline again follows the body surface. Note that, according to the above discussion, the sonic line should be normal to the lower surface at the nose and then run forward and upward around the nose. The above features of the flow near the wedge nose are shown in exaggerated form in Sketch 4b, but they are omitted in the other figures.

The flow pattern is shown at a higher angle of attack in Sketch 4c. The separation at the nose is assumed to be only local. The nose supersonic region is now enlarged, and the lower surface supersonic zone behind the wedge shoulder is reduced in size. The supersonic zone,

behind the wedge shoulder on the upper surface, has grown so that the terminating shock no longer intersects the body surface. The flow is now supersonic on the upper side at the trailing edge and is at a lower pressure than the flow from the lower surface near the trailing edge. Thus, the flow along the lower surface is accelerated with a sonic line appearing on the lower surface at the trailing edge. The sonic line runs from the trailing edge to the terminating shock so that the supersonic zone is again enclosed. Weak oblique shocks arise at the trailing edge in order to make the flow behind the trailing edge approximately parallel and at small downwash angle.

At a larger angle of attack, again assuming only local separation at the nose, the flow is that shown in Sketch 4d. The nose supersonic zone has increased in size until it merges with the supersonic zone behind the upper shoulder of the wedge. The terminating shock for the nose supersonic zone is no longer necessary, and the flow over the upper surface is entirely supersonic. On the lower surface, the supersonic zone behind the shoulder is further reduced in size. The flow pattern at the trailing edge does not differ from the previous pattern, Sketch 4c. The flow of Sketch 4d is essentially the pattern one would expect to find over a flat plate at high subsonic speeds.

Note that at $M_\infty = 1$, a double wedge has $C_L \sim \alpha^{2/3}$, if $\alpha/(t/c) \gg 1$ (Ref. 6). This result, $C_L \sim \alpha^{2/3}$, is also true for a flat plate at $M_\infty = 1$, since $\alpha/(t/c) \rightarrow \infty$ even for small α . This result, from similarity arguments, provides a check on the above flow pattern arguments.

The above flow patterns at large angles of attack may not actually

be obtained if the flow separates completely at the nose or behind the wedge shoulders. However, the above qualitative discussion should aid in giving an understanding of the results obtained later by experiment. This is particularly true at high subsonic free stream Mach numbers where analytical solutions for lifting bodies are very difficult.

III. DESCRIPTION OF AIRFOILS AND EXPERIMENTAL TECHNIQUES

From the discussion of flow patterns over a double wedge (Section II), it should be clear that an important feature of the flow at transonic speeds over lifting profiles is the existence and growth of local supersonic regions adjacent to the profile surface. When the present investigation was initiated, the importance of the local supersonic regions with their associated terminating shocks was recognized, and the experimental program was conducted accordingly.

1. Description of Airfoils

Only symmetrical profiles were tested in the present investigation. The following three basic profiles were investigated.

A. Truncated Wedge

The truncated wedge profile was simply the forebody of a double wedge. The profile dimensions are shown in Fig. 1. The flow over the truncated wedge will be essentially the same as that over the forebody of a double wedge (Section II). At transonic speeds, the sonic lines will emanate from the rear of the body on both upper and lower surfaces and will run to a terminating shock behind the body. The only supersonic zone on this profile will occur near the nose when the body is at a small angle of attack. Thus, one would expect the surface pressure distribution to change smoothly with Mach number and angle of attack, if the angle of attack is small enough to minimize the effect of the nose expansion region.

B. Round Nose Airfoil

This profile represents an extreme case where the maximum

thickness is reached very near the nose. The profile dimensions are shown in Fig. 1. At transonic speeds the flow over the round nose airfoil will always be supersonic near the nose if the free stream Mach number is high enough. Sonic lines will originate on the round nose and run back to terminating shocks which may or may not be on the airfoil, depending on the angle of attack and Mach number. The flow over this profile will be essentially similar to that over the rear half of the double wedge (Section II).

C. Double Wedge

The flow over this profile has already been discussed (Section II). One profile had a thickness ratio of 0.054, and the other was approximately twice as thick. The profile dimensions are again shown in Fig. 1. The double wedges and the truncated wedge had a nose radius of approximately 0.0003 inches.

2. Experimental Technique and Apparatus

A. Measurement of Lift Forces and Moments

There are a number of well-known experimental techniques which can be used to determine the lift and moment characteristics of airfoils in wind tunnels. These techniques include direct balance measurements, integration of static pressure along the tunnel walls, interferograms of the flow field about the airfoil, and conventional static pressure measurements on the airfoil surface. All of these methods were considered at the beginning of the present investigation. Each had certain disadvantages which are described below.

A balance gives only integrated values of forces or moments and

little detailed information about the flow field around an airfoil. Since the present investigation was intended to be mainly descriptive, a balance was not considered desirable or at any rate efficient.

Static pressure measurements on the tunnel walls also give little information about the flow field around an airfoil. In addition, they are subject to large tare corrections so that small changes in lift or moment are difficult to detect. Furthermore, extensive instrumentation is required.

Interferometric techniques seem very desirable since one can obtain a quantitative description of the entire flow field about an airfoil with one picture. Unfortunately, the least increment in density and hence pressure that the GALCIT interferometer (Ref. 16) can detect is quite large when one wishes to obtain small changes in lift or moment. This need not be the case for all interferometers, since the sensitivity increases with tunnel width, air density, and light frequency (Ref. 1).

Conventional static pressure taps on the airfoil surface give more detailed information about the flow field than can be obtained with a balance or by static pressure measurements on the tunnel walls. In order to minimize wind tunnel wall effects, the airfoils used in the present investigation were necessarily small. With airfoils of small thickness ratio and chord, it was found to be quite difficult to include sufficient piping inside the airfoil to measure the entire pressure distribution.

A reasonable solution to the above difficulties was found. The method finally adopted consisted of two slender static pressure probes which could be traversed over the upper and lower airfoil surfaces. The probes were made of stainless steel tubing through which pressure sensing

holes were drilled parallel to the airfoil surface and approximately two inches downstream of the conical probe tips.

A description of the probes and the probe calibration procedure is given in Appendix B. Fig. 2 shows a schematic drawing of the probe dimensions and arrangement on a thin airfoil. The calibration of the probes showed that the surface pressure could be measured with precision on flat surfaces and even near a corner formed by the intersection of two flat surfaces. The method failed, however, near a stagnation point, for example, the nose of a wedge. The failure was not considered detrimental for the present investigation, since the errors were confined to a small region near the nose. As a matter of fact, one has the same difficulty with conventional surface pressure taps which are difficult to install very near a sharp nose.

B. Description of Tunnel and Tunnel Calibration

The experiments were performed in the GALCIT 4- x 10-inch Transonic Wind Tunnel. A description of the tunnel and flexible nozzle is given in Ref. (17). The flexible nozzle can be adjusted to give a uniform supersonic flow in the test section. For subsonic flow, the second throat area was reduced until the test section Mach number became subsonic. The flexible nozzle was then flattened to give a uniform subsonic flow in the test section. The subsonic Mach number was varied by changing the second throat area.

The static pressure in the tunnel was measured for calibration by inserting a 12-inch diameter aluminum "window" in the tunnel wall at the test section. The "window" was fitted with a number of surface pressure taps. For subsonic calibration, eight static pressure taps

were also installed in the tunnel wall upstream of the test section "window".

After calibration, the model was installed and tested. At supersonic speeds the model should introduce no upstream disturbances. At subsonic speeds the upstream disturbances were appreciable and changed with angle of attack. Accordingly, the pressures from the eight tunnel wall taps, ahead of the test section, were displayed on a multiple mercury manometer so that the decay of the upstream influence of the model could be determined. With the models used in the present investigation, it was always possible to measure the undisturbed free stream velocity at one or more of the eight upstream static pressure taps.

C. Probe and Airfoil Mounting and Instrumentation

The two-dimensional airfoils were mounted from wall to wall across the four inch width of the Transonic Tunnel. The airfoils were wider than the tunnel width so that each end could be clamped in mounting plugs. The plugs were inserted into recesses in twelve inch diameter solid steel "windows" flush with the tunnel walls at the test section.

The steel windows on each side of the tunnel were fastened together by a rigid bracket extending around the tunnel. The airfoil angle of attack could then be changed by rotating the steel windows as a unit. The angle of attack was indicated by a vernier scale to an accuracy of ± 5 minutes of arc. The sliding surface pressure probe was passed through one of the steel "windows" behind the airfoil and extended forward to the airfoil surface as shown in Fig. 2. A picture of a double wedge airfoil and the sliding probe mounted in the wind tunnel are shown in Fig. 4. In Fig. 4 the airfoil mounting plug and "window" have been

removed from the near side of the airfoil.

The deflection of the thin airfoils due to spanwise bending was considerably reduced by the airfoil mounting method which made the airfoil and tunnel walls an integral unit. Since the airfoil passed through the tunnel walls, upwash flow through gaps near the walls did not occur. However, the flow over the airfoil was not strictly two-dimensional since the ends of the airfoil were immersed in the side wall boundary layer. Bryson (Ref. 1) has found that approximately two-dimensional flow over symmetrical models at zero angle of attack can be obtained by leaving gaps of the order of the boundary layer momentum thickness between the tunnel wall and model. This procedure was not considered practical due to gap effects and mounting difficulties. The effect of the flow disturbances due to airfoil mounting is discussed at the beginning of Section IV.

The probe pressures were measured by two mercury micromanometers accurate to ± 0.02 cm. Hg. One manometer measured the pressure difference between the upper and lower surface probes, and the other measured the difference between the lower probe and free stream static pressure.

Schlieren pictures of the flow over the airfoils using a spark light source and horizontal knife edge were also made. After the surface pressure tests were completed, the ends of the airfoils were cut off so that they just spanned the tunnel. The steel "windows" were replaced with glass windows, and the airfoils were supported on the lower surface by two internal struts running downstream along each side of the tunnel. The complete upper surface and portions of the nose and trailing edge were then visible for schlieren pictures.

IV. EXPERIMENTAL RESULTS

In this section the results of the experiments on the three basic airfoil shapes (Fig. 1) will be discussed. The results include schlieren pictures of the flow, pressure distribution measurements, lift forces, and locations of center of pressure.

Unfortunately, no measurements at supersonic free stream Mach numbers with a detached bow wave were possible with the method of airfoil mounting used in this investigation. As was mentioned previously, the model completely spanned the tunnel so that each end of the airfoil was immersed in the side wall boundary layer. At supersonic speeds, the interaction of the bow shock wave and the side wall boundary layer caused a large deviation from two-dimensional flow. In particular, it was observed that the bow shock detached from the nose of a wedge model at much higher Mach numbers than predicted by exact shock theory. Even with an attached bow shock wave, it was observed that large pressure disturbances originated at the intersection of the airfoil leading edge and the side walls of the tunnel. These disturbances caused a large change in the pressure distribution over the rear half of the airfoil on the tunnel center line. Consequently, measurements at supersonic free stream Mach numbers were not attempted.

At subsonic speeds, however, the above difficulties were not encountered. As a matter of fact, the sharpness of the shock waves which intersect the airfoil surface (Figs. 6, 10, 13, and 17) indicates that the flow was approximately two-dimensional at subsonic free stream Mach numbers. The results obtained at subsonic speeds will now be

discussed.

1. Truncated Wedge

The flow field over the truncated wedge may be expected to be qualitatively similar to the flow field over the forebody of a double wedge, since the sonic line will be fixed at the wedge shoulder. However, the shoulder expansion on the truncated wedge cannot be accomplished without flow separation. Thus, at zero angle of attack and low subsonic speeds the shedding of vorticity at the shoulder gave rise to a vortex street in the wake behind the airfoil (Fig. 5, $M_\infty = 0.773$). The sound waves generated by this process could not penetrate into the small supersonic zone above and behind the wedge shoulder (Fig. 5).

At higher speeds and zero angle of attack (Fig. 5, $M_\infty = 0.812$, 0.838 , and 0.852) the supersonic regions grew in size, and the associated terminating shock moved downstream. At $M_\infty = 0.852$, the vortex street has probably disappeared, and a "dead air" region exists behind the truncated wedge.

At an angle of attack a supersonic region due to flow expansion around the nose appeared. This region grew in size with increasing free stream Mach number as shown in Fig. 6.

Since the only shock wave on the airfoil surface was that terminating the nose supersonic region, one might expect a smooth variation of lift curve slope with Mach number for small angles of attack. Such was found to be the case when the pressure distribution measurements were integrated and plotted in similarity form (Fig. 7).

Note that the similarity parameters used are those advocated by

Spreiter (Ref. 6) and are based on the assumption that lift is a linear function of angle of attack for small angles. The assumption of linearity was found to be good up to angles of attack of approximately two degrees for $M_\infty \approx 0.90$. Of course, the lift curve was linear for greater angles of attack at lower Mach numbers.

In Fig. 7, and those following, the vertical bars on the experimental points indicate the estimated error of measurement. Also shown for comparison are the results of Eggers (Ref. 18). It can be seen that the similarity rules advocated by Spreiter do reduce the lift curve slope for similar airfoils of different thickness ratios, to a common curve.

Also shown on Fig. 7 are a number of theoretical results. As discussed previously, at sonic or supersonic speeds the limiting Mach wave "isolates" the rear half of a double wedge from the front half. Using this concept, the double wedge results of Guderley and Yoshihara (Ref. 8) and Vincenti and Wagoner (Ref. 9) have been plotted for the wedge forebody at sonic and supersonic speeds. Also included are the results from transonic shock expansion theory above the bow shock attachment Mach number. Using the stationarity principle at $M_\infty = 1$, it can be seen (Fig. 7) that there is a smooth transition between the experimental subsonic and theoretical supersonic results.

At subsonic speeds (Fig. 7), the Prandtl-Glauert rule for the lift curve slope in an unbounded flow is plotted for comparison with the Prandtl-Glauert result of Tsien and Lees (Ref. 19) for flow between walls using the actual tunnel and airfoil dimensions. Since the difference between these curves was small, it was concluded that the tunnel wall corrections could be ignored, at least at low subsonic speeds. No

attempt was made to correct any of the data for the presence of the tunnel walls even when the Mach number approached the choking Mach number. Admittedly, the results are affected by the presence of the tunnel walls. However, the lack of a wall correction theory, when shocks are present in the flow at high speeds and the small corrections at lower speeds, makes use of the uncorrected data plausible at low speeds and necessary at higher speeds. Another method for accounting for wall effects requires testing with similar, but different size models, and extrapolating to zero size, which would be equivalent to letting the tunnel walls recede infinitely far from the airfoil. This procedure was not attempted since the lift at subsonic speeds would be greatly affected by the low Reynolds number ($R/\ell \approx 3 \times 10^5/\text{in.}$) of the flow in the Transonic Tunnel.

The last theoretical result, appearing as a dashed line on Fig. 7, is an approximate computation for the lift of the truncated wedge at subsonic speeds. The complete computation is carried out in Appendix C, but the results will be interpreted here.

The computation was done in the hodograph plane, where the transonic equations (Ref. 4) are linear, assuming the lifting solution to be a small perturbation to the zero angle of attack solution given by Cole (Ref. 20). The boundary conditions were the usual flow tangency conditions on the wedge surface with a uniform free stream far ahead of the body and a stagnation point on the nose. At the wedge shoulder, the velocity was assumed to be sonic for $0 < M_\infty \leq 1$. Cole's solution was obtained without specifying conditions on the sonic line and also ignores, when $M_\infty < 1$, the upstream influence of the flow downstream of the

supersonic regions. Thus, the present computation, which is a small perturbation of Cole's solution, gives zero lift as $M_\infty \rightarrow 0$, because an effective "Kutta condition" for this blunt trailing edge body (that is, the upstream influence of the downstream flow) has not been included. In fact, a solution for the lift of bodies with a cut-off trailing edge is not yet possible due to a lack of knowledge of flow separation at bluff ends (that is, the base pressure problem).

There is, however, some interest in the present lifting solution since it does not include a condition analogous to the Kutta condition. In particular, at Mach number one the solution for the lift curve slope is only 10 percent lower than the more exact result of Guderley and Yoshihara (Ref. 8). The error arises because the boundary conditions on the sonic line, which can be obtained from the influence of the shoulder expansion on the flow at the sonic line (Ref. 13), were not satisfied. However, at Mach number one a "Kutta condition" is not necessary, since the flow downstream of the limiting Mach wave cannot influence the upstream flow.

As $M_\infty \rightarrow 0$ the supersonic zone behind the wedge shoulders decrease in size and the upstream flow field is no longer independent of the flow downstream. Since no "Kutta condition" was included in the present computation, the lift gradually decreases to zero, as $M_\infty \rightarrow 0$. The actual smooth transition from classical incompressible flow, with the inclusion of a Kutta condition, to transonic flow which at $M_\infty = 1$ requires no Kutta condition, has thus been demonstrated by the present experiments.

Fig. 8 shows the location of the center of lift on the truncated

wedge at small angles of attack, $\alpha < 2^\circ$, as a function of the reduced Mach number. If the local pressure difference across the airfoil is linear in the angle of attack, so are the lift and moment. The center of lift will thus be independent of the angle of attack. As a matter of fact, the location of the center of lift did not change appreciably when α was varied at constant M_∞ . In addition, the center of lift was not greatly affected by changes in M_∞ . However, the location of the center of lift as $M_\infty \rightarrow 1$ does not go over smoothly to the sonic and supersonic theoretical results, whereas the lift curve slope did check the theory for $M_\infty \rightarrow 1$. The discrepancy is believed to be due to the difference in the "rounding off" of the upper and lower wedge shoulders by the boundary layer. Thus, the sonic line was located farther forward on the upper surface than the lower. Therefore, an increment of lift occurred at the wedge shoulder and moved the center of pressure rearward. Without viscosity, the pressure difference between the upper and lower wedge surfaces will be zero at the shoulder, since sonic velocity can be attained only at that point.

The lift and location of center of pressure for large angles of attack, at $M_\infty = 0.841$, are shown in Fig. 9. The lift was not a linear function of angle of attack for $\alpha > 2^\circ$. The rapid growth of the nose supersonic region and consequently lower pressure on the upper wedge surface accounts for the non-linear increase in lift. At larger angles of attack, $\alpha > 6^\circ$, the nose supersonic region grew and made the flow supersonic over the entire upper surface (discussed in Section II). The pressure on the upper surface then changed less with angle of attack than before, and the slope of the lift curve decreased as shown in

Fig. 9. Flow separation from the leading edge may have been partially responsible for the decrease in lift at high angles of attack. Unfortunately, no check for flow separation was made.

The behavior of the center of lift for large angles of attack is also shown in Fig. 9. Here the growth of the nose supersonic region shows up as a shift in center of lift toward the nose when $2^\circ < \alpha < 5^\circ$. At higher angles, the increased size of the nose supersonic zone and possible separation caused the center of lift to move rearward slightly behind its former location.

2. Round Nose Airfoil

The flow field over the round nose airfoil, abbreviated by R.N.A., will be completely different from the flow over the truncated wedge. The point of maximum thickness is reached on the R.N.A. very near the nose. At the critical Mach number, sonic velocity will be attained at the point of maximum thickness very near the nose. Above the critical Mach number sonic lines will emanate from the round nose, and the approximately normal shocks which terminate the nose supersonic regions on each side of the airfoil will intersect the airfoil surface. As $M_\infty \rightarrow 1$, the terminating shocks will move downstream off the airfoil. The R.N.A. flow patterns will thus be qualitatively similar to those over the rear half of the double wedge (Section II).

Schlieren pictures of the flow over the upper surface of the R.N.A. are shown in Fig. 10. Three of the photographs were taken at zero angle of attack for increasing free stream Mach numbers. At $M_\infty = .803$, small nose supersonic zones have just appeared. The normal shocks

which terminate the small supersonic zones caused the boundary layer to separate locally and then reattach. After reattachment the boundary layer was much thicker. An impact pressure probe traversed chordwise along the airfoil surface was used to ascertain that the boundary layer did reattach. When the boundary layer was locally separated under the normal shock, the impact pressure probe read the local static pressure near the point of separation. After reattachment the impact pressure read by the probe was 3 to 5 cm. Hg. higher than the local static pressure. The probe opening was rectangular, approximately 0.002×0.020 inches, with the center of the opening within 0.003 inches of the surface.

At higher Mach numbers the nose supersonic region grew rapidly until at $M_\infty = 0.915$ (Fig. 10) the terminating shocks moved off the airfoil and were downstream out of the field of view. Local separation under the normal shocks on the airfoil surface was not as severe at Mach numbers above $M_\infty = 0.803$ as it was at $M_\infty = 0.803$, even with the airfoil at an angle of attack. In the last picture of Fig. 10 ($M_\infty = 0.897$, $\alpha = 0.2^\circ$) the change in size of the upper and lower supersonic zones should be compared with the picture taken at zero angle of attack at the same Mach number. It can be seen that a small change in angle of attack had a very large effect on the flow field.

In Fig. 11, the lift coefficient is shown as a function of angle of attack for six free stream Mach numbers. At low speeds, the lift was a linear function of angle of attack. At higher speeds, non-linear effects began to appear. The non-linear behavior of lift coefficient was caused by the non-linear growth and shrinkage of the upper and lower

supersonic regions and was not due to flow separation. When the Mach number was increased to higher values, the terminating shocks moved off the airfoil surface leaving the flow supersonic on each side. At these speeds the lift coefficient was again a linear function of angle of attack, but considerably lower lift was developed. Large values of $dC_L/d\alpha$ near $\alpha = 0$ were obtained at $M_\infty \approx 0.90$, where the size of the supersonic zone was very sensitive to changes in angle of attack (see Fig. 10 $M_\infty = 0.897$, $\alpha = 0^\circ$ and 0.2°). The behavior of the lift curve slope for the R.N.A. as a function of M_∞ is compared with the other airfoils in the summary at the end of this section.

Fig. 12 shows the location of the center of lift for the R.N.A. as a function of angle of attack at different Mach numbers. At low speeds the center of lift was independent of α and was located near the quarter chord point. As the Mach number increased to $M_\infty \approx 0.80$, the center of lift moved forward to the two-tenths chord point but was still independent of α . At the above speed an increased increment of lift due to the difference in size of the supersonic regions near the nose accounted for the forward movement of the center of lift. The fixed location of the center of lift was due to the linear growth and shrinkage of the small nose supersonic regions when the angle of attack was changed.

At higher speeds the growth and shrinkage of the supersonic regions were no longer linear in α . From the plot it can be seen that at constant M_∞ the center of lift moved progressively rearward as the relative size of the upper and lower supersonic regions changed with increasing angle of attack. It can also be seen that at constant angle of attack the center of lift moved to approximately mid-chord when M_∞

increased. Finally, at $M_\infty = 0.918$, the terminating shocks were downstream of the airfoil surface, and the center of lift was located at 55 percent chord and was not dependent on the angle of attack.

The lift characteristics of the truncated wedge and the R.N.A. were completely different due to the presence of supersonic flow and shock waves on the surface of the R.N.A. and the absence of supersonic flow on the truncated wedge surfaces. The double wedge, which has both subsonic and supersonic surface velocities, will be discussed in the next section.

3. Double Wedges, $t/c = 0.054$ and 0.104

Since the flow field over the double wedge has already been discussed (Section II), the schlieren pictures can be considered immediately. The first three pictures of Fig. 13 show the flow over the thinner double wedge at zero angle of attack. At $M_\infty = 0.805$ a small supersonic zone originated at the wedge shoulder. The terminating shock again caused local separation which was checked with the impact pressure probe as described in Part 2 of this Section. The boundary layer on the wedge afterbody, downstream of the local separation point, was much thicker than on the wedge forebody. At a higher Mach number, $M_\infty = 0.879$, the supersonic regions grew larger, but the shocks still caused local boundary layer separation with a thicker boundary layer downstream of the shock. Finally, at $M_\infty = 0.913$ the shocks were downstream out of the field of view, and the boundary layer was not locally separated or as thick as it had been.

The last picture of Fig. 13 shows the thin double wedge at an

angle of attack. All the characteristic features of the flow field, discussed in Section II, are visible, even though the boundary layer was still locally separated under the shock wave. Two of the pictures ($M_{\infty} = 0.879$, $\alpha = 1.5^{\circ}$ and $\alpha = 0^{\circ}$) should be compared. At an angle of attack, $\alpha = 1.5^{\circ}$, the local separation under the shock appears different from the separation at zero angle of attack. Apparently, the boundary layer was turbulent at $\alpha = 1.5^{\circ}$, since the flow over the sharp wedge nose "trips" the boundary layer. The tripping effect of the flow over a pointed nose was mentioned by G. P. Wood of the Langley Aeronautical Laboratory in a private communication. The effect was also substantiated by the experiments on the $t/c = 0.104$ double wedge, and it will be described in the following pages.

Fig. 14 shows schlieren pictures of the flow over the thicker double wedge, $t/c = 0.104$, at low and high Mach numbers and zero angle of attack. The boundary layer on the afterbody of the wedge was very thick, but not separated, at $M_{\infty} = 0.730$ (Fig. 14). At higher speeds, the shocks terminating the supersonic zone caused complete separation of the flow over the afterbody. This case will be discussed later. Finally, when $M_{\infty} = 0.878$ (Fig. 14) the terminating shocks were downstream off the airfoil, and the boundary layer was not separated.

A. Double Wedge Results. Only Local Separation

Throughout the Mach number range the lift curve slope of the thin wedge was linear in an angle of attack for $0^{\circ} < \alpha < 2^{\circ}$. The thicker double wedge also showed a linear variation of lift curve slope at low and high Mach numbers where the flow did not separate completely. Since the lift was linear in α , the results for the lift of the double

wedges have been plotted in Fig. 15, using the transonic similarity parameter (Ref. 6). Also included are the experimental results of Bartlett and Peterson (Ref. 21) for a 10 percent thick double wedge at the same Reynolds number as the present experiments, $R/\ell \approx 3 \times 10^5/\text{in.}$

At low speeds the lift curve slope for the wedges (Ref. 15) was considerably lower than the Prandtl-Glauert value based on the classical incompressible result, $C_L = 2\pi\alpha$. The low values of $dC_L/d\alpha$ were due to the thick boundary layer which lowered the airfoil efficiency. However, as the Mach number was increased, the slope of the lift curve increased in accordance with the Prandtl-Glauert rule until at $\xi_\infty \approx -1$, $dC_L/d\alpha$ decreased abruptly to approximately the value computed by Guderley and Yoshihara (Ref. 8). The subsonic experimental points thus appear to fair smoothly into the theoretical results for $M_\infty \geq 1$. Note that the thicker boundary layer on the 10 percent thickness ratio wedge had a considerable effect on the lift curve slope so that the similarity rules were not followed very well at low speeds. However, at the highest speeds attainable without choking, the shock waves were off the airfoil, and the boundary layer was apparently thin enough to allow the similarity rules to be followed.

The above drop in lift at $\xi_\infty \approx -1$ was not due to separation or stalling but was due to the formation of supersonic zones behind the shoulder which grew rapidly as $\xi_\infty \rightarrow -1$. Near $\xi_\infty = -1$ the terminating shocks moved off the airfoil, and the flow over the rear portion of the wedge was supersonic. As was found with the truncated wedge at large α and with the R.N.A., the double wedge was less efficient in the production of lift when the flow over it was supersonic. Thus, the

supersonic flow over the rear half caused the decrease in lift near $\xi_{\infty} = -1$. Note that only half of the airfoil was supersonic, so that the decrease in lift was not as great as the decrease found on the R.N.A (Fig. 24).

The location of the center of lift is shown in Fig. 16. The center of lift was located at approximately 1/4 chord at low speeds. As the Mach number was increased, the center of lift moved rearward to 40 percent chord and then forward toward the value given by Guderley and Yoshihara for $M_{\infty} = 1$.

The center of lift travel can be explained in a manner similar to that for the R.N.A. Near $\xi_{\infty} \approx -1$, the change in size of the supersonic zones over the rear portion of the wedge was quite sensitive to changes in α . Thus, near $\xi_{\infty} \approx -1$, larger increments in lift occurred on the rear portion of the wedge than at lower subsonic speeds so that the center of lift moved rearward. At higher speeds the supersonic zones had grown and included the entire rear half of the wedge so that the consequent decrease in lift over the wedge afterbody shifted the center of lift forward again.

The location of the center of lift was not dependent on α for the 10.4 percent thick double wedge when the flow was not separated (that is, at low and high M_{∞}). The center of lift on the 5.4 percent thick double wedge was also independent of α except at high subsonic speeds, $0.90 < M_{\infty} < 0.92$, when the terminating shocks were no longer on the wedge afterbody. When $0.90 < M_{\infty} < 0.92$ the center of lift on the 5.4 percent thick wedge moved forward as the angle of attack was increased. Thus, although the lift was linear in α , the moment was

non-linear. The forward shift was caused by the very strong expansion over the upper surface near the nose. It is interesting that there were deviations from linear behavior at angles of attack which were less than the wedge-nose semi-angle (3°).

B. Double Wedge Results. Separation on the Wedge Afterbody

As mentioned above, the flow over the afterbody of the 10.4 percent thick double wedge separated completely under the shocks for approximately $0.75 < M_\infty < 0.87$. In Fig. 17, schlieren pictures of the flow over the wedge are shown for the Mach number ($M_\infty = 0.848$) at which the effects of separation were the greatest. The two pictures labeled "no rake" for $\alpha = 0^\circ$ and $\alpha = 1^\circ$ will be considered first. At $\alpha = 0^\circ$ the separation points on the upper and lower surfaces were approximately symmetrical. The separation was apparently laminar and similar to the less severe separation which occurred on the 5.4 percent thick double wedge (Fig. 13, $M_\infty = 0.879$, $\alpha = 0^\circ$). At $\alpha = 1^\circ$, the separation was apparently turbulent on the upper surface and again similar to the less severe separation shown in Fig. 13 ($M_\infty = 0.879$, $\alpha = 1.5^\circ$) for the 5.4 percent double wedge.

The important effect of separation on the flow field over the 10.4 percent thick wedge (Fig. 17) will now be discussed. It can be seen that the upper surface supersonic zone grew smaller as α was increased, instead of larger as one would expect, while the size of the lower surface supersonic zone did not change appreciably. Thus, the flow separation was severe enough to effectively alter the airfoil shape and hence the flow field when the angle of attack was increased.

Fig. 18 shows the pressure distribution measured by the static

probes for $\alpha = 2.3^\circ$ at $M_\infty = 0.848$. The forebody of the wedge carried lift as indicated by the "+" sign while the afterbody carried negative lift as shown by the "-" sign. It can be seen from the schlieren pictures (Fig. 17) and pressure distribution (Fig. 18) that the flow over the afterbody was supersonic (low pressure) over a large portion of the lower surface. The pressure was much higher, due to separation, over most of the upper afterbody surface. Thus, a large increment of negative lift was developed on the afterbody. The net lift obtained from the pressure distribution shown in Fig. 18 was actually negative, $C_L = -.022$.

Fig. 19 shows the lift coefficient as a function of angle of attack for different Mach numbers. From the figure, it can be seen that the effects of separation became more severe as the supersonic regions grew in size when the Mach number increased from $M_\infty = 0.730$ to $M_\infty = 0.848$. With a further increase in Mach number, $M_\infty = 0.848$, the supersonic zones grew larger and the separation effects decreased until, at $M_\infty = 0.888$, the shock waves were no longer on the airfoil and the lift was again linear in α . The phenomenon of negative lift caused by separation at high subsonic speeds is not new. For instance, Göethert (Ref. 3) reported negative lift forces on NACA 0-00xx symmetrical airfoils at high subsonic speeds in 1942. Göethert concluded that flow separation was the cause of negative lift, and he showed that the effect of separation was intensified as the airfoil thickness ratio increased.

Göethert's results were obtained for Reynolds numbers greater than 2.2×10^6 , whereas the Reynolds number of the present experiments was 6×10^5 , based on the airfoil chord. The present Reynolds

number could not be greatly increased; however, tests were made to ascertain that flow separation would still occur if the boundary layer were turbulent.

The boundary layer was tripped by a "rake" or "fence" cemented on the nose of the double wedge. The "rake" consisted of many short lengths of wire of 0.006 inch diameter cemented to the airfoil's upper and lower surfaces near the nose and projecting upstream 1/16 inch. After the cement had hardened the wires were bent around the nose so that they were normal to the upper and lower surfaces. The wires were spaced approximately 1/16 inch apart along the airfoil span.

Fig. 17 (rake, $\alpha = 0^\circ$ and 1°) shows the flow over the wedge with the rake in place. On comparing the $\alpha = 0^\circ$ pictures with and without the rake, it can be seen that the flow separation has changed character. It seems clear that the boundary layer was laminar for no rake, $\alpha = 0^\circ$, and turbulent with the rake. This conclusion is also supported by the well-known qualitative result (Ref. 22) that upstream effects for shock-wave boundary-layer interaction are greater if the boundary layer is laminar. Thus, with no rake the boundary layer was appreciably thickened well ahead of the shock-wave interaction point (Fig. 17, $\alpha = 0^\circ$). With the rake, the upstream influence through the boundary layer was smaller (Fig. 17, $\alpha = 0^\circ$).

Qualitative results for the lift of the double wedge with and without the rake are shown in Fig. 20, where it can be seen that the effect of the rake was considerable. Without the rake, $dC_L/d\alpha$ was positive at $\alpha = 0^\circ$ and only became negative for $\alpha \approx 0.7^\circ$. With the rake installed, $dC_L/d\alpha$ was negative for $0^\circ < \alpha < 1^\circ$. Since the rake both tripped and

thickened the boundary layer, the effect of tripping alone could not be determined from the tests with the rake. However, the rake did make the boundary layer turbulent on both the upper and lower surfaces for all small angles of attack. Without the rake, the boundary layer was always laminar on the lower surface and changed from laminar to turbulent on the upper surface as α was increased.

The non-linear lifting effects shown in Fig. 19 and Fig. 20 were caused by increments of negative lift acting on different portions of the afterbody surface. As one might expect, the location of the center of lift was greatly affected by separation. The actual values measured for the double wedge, at different Mach numbers, have not been shown since the location of the center of lift was greatly influenced by the low Reynolds number of the flow. As an illustration of the effect of separation on the center of lift, Fig. 21 shows the location of the center of lift at $M_\infty = 0.848$ with and without the rake. The large positive and negative location of the center of lift without the rake was caused by the net lift passing through zero. This may be readily understood from the equation for the location of the center of lift, $x/c = C_m/C_L$. The lift was positive on the forebody and negative on the afterbody, so that C_m was approximately constant. However, as C_L passed through zero, the location of the center of lift went to large positive and negative values.

The changes in center of lift were striking and should indicate the difficulties a pilot would have when flying an airplane at high speeds with separation on the wings or control surfaces. One possible effect will be mentioned. With either a laminar or turbulent boundary layer, negative lift was obtained on the afterbody of the wedge for small α . With

an increase in angle of attack to larger values, the afterbody lift would eventually become positive. If the afterbody was used as an elevator, rudder, or aileron, a forced oscillation of the control surface could be established by the negative lift increments on the rear portion of the airfoil. The oscillation would be limited in amplitude by the positive lift occurring at large α . As a matter of fact, Göethert (Ref. 23, p. 42) investigated separation effects due to the deflection of a flap mounted on an NACA 0-0009 airfoil at zero angle of attack. His results showed that at high speeds the flap forces were negative for small flap deflections and became positive for larger flap angles. Thus, a "limit cycle" oscillation of a control surface seems quite possible. The oscillation of control surfaces would be an interesting and important problem for further research.

4. Summary of Lift and Drag Results

In Fig. 22, the lift curve slope at zero angle of attack for the three basic profiles has been plotted as a function of Mach number. The differences between the curves were due almost entirely to the different locations of the point of maximum thickness. In other words, the different results were due to the varying amounts of supersonic flow adjacent to the airfoil surfaces. Thus, the truncated wedge, with maximum thickness at the trailing edge, had only the small, supersonic nose expansion zone on the surface. The lift curve slope was a monotonic increasing function of Mach number for $M_\infty < 1$.

The double wedge surfaces had partially supersonic flow over the afterbody at high subsonic speeds. $dC_L/d\alpha$ increased according to

the Prandtl-Glauert law up to the Mach number at which the supersonic zones and their terminating shocks began to move over the wedge afterbody. As the Mach number increased, $dC_L/d\alpha$ increased still further and then decreased as the shocks passed off the afterbody.

The R.N.A. had supersonic flow over almost the entire surface. The behavior of $dC_L/d\alpha$ was qualitatively similar to the double wedge, but the peak in $dC_L/d\alpha$ was much greater. The large peak was partially due to the small thickness ratio of the airfoil but probably would not have been as great if it had been a double wedge of the same t/c . A double wedge with $t/c = 0.033$ would have $\tilde{C}_L/\alpha \approx 5$ (Fig. 15), so that $dC_L/d\alpha \approx 12$. Whereas, the R.N.A. had $dC_L/d\alpha \approx 33$. Unfortunately a double wedge with $t/c \approx 0.03$ was not tested.

Drag coefficients for the truncated wedge and the double wedges are shown in Fig. 23. The truncated wedge had the same maximum thickness as the $t/c = 0.104$ double wedge. The truncated wedge drag was much higher, due to the low pressure on the base of the airfoil. (The base pressure was measured by a tap at the center of the base and was assumed constant over the entire base.) Note that D'Alembert's paradox ($C_D \rightarrow 0$ as $M_\infty \rightarrow 0$) was approximately true for the double wedges, but of course it does not apply to the truncated wedge where the flow separates at the base.

From the above lift and drag results one can see that the favorable lift characteristics of the truncated wedge at high subsonic speeds are offset by high drag coefficients at low subsonic speeds. Actually, at higher Reynolds numbers, of the order of 4×10^6 , the lift coefficient of the truncated wedge might be increased to as much as

50 percent more than the values herein reported, since other airfoils have $C_L > 2\pi$ at low speeds when a substantial portion of the trailing edge is cut away (Ref. 24). However, the variation of C_D with Reynolds number for the truncated wedge must be investigated before definite conclusions can be reached.

The last figure, Fig. 24, shows the good agreement for the drag of the double wedges when plotted in similarity form. Note that the points obtained with laminar separation on the afterbody of the thick wedge have been included. The separation occurred when the drag was rising rapidly. Therefore, the effect of separation does not show up well on this plot.

V. CONCLUSIONS

After investigating the lift characteristics at subsonic speeds of the three basic, two-dimensional profiles, the following conclusions can be drawn:

1. The surface pressure distribution can be measured with good accuracy by a conventional static probe if the airfoil thickness ratio is small. The method should have application to other bodies which are difficult to instrument with surface pressure taps.

2. For the three basic profiles, the lift coefficient is a linear function of angle of attack when $\alpha \ll t/c$ with the following exceptions:

a) Non-linear effects appear when a substantial amount of flow separation takes place.

b) If the airfoil profile has its maximum thickness near the leading edge, non-linear effects appear for free stream Mach numbers where the shock waves terminating the supersonic zones move rapidly with α over the airfoil surface. At higher Mach numbers the shocks move downstream off the airfoil, and the lift is again linear in α .

3. The slope of the lift curve, for $\alpha = 0$, is a monotonic increasing function of free stream Mach number for profiles with no supersonic zones on the airfoil surface. With supersonic flow on a portion of the surface, a maximum value of $(dC_L/d\alpha)_{\alpha=0}$ is reached between the critical Mach number and the Mach number at which the shocks terminating the supersonic zone move off the airfoil. The maximum value of $(dC_L/d\alpha)_{\alpha=0}$ increases when the location of the sonic line is

moved toward the leading edge by shifting the location of maximum thickness forward.

4. Severe flow separation caused by the shocks terminating the supersonic zone is to be expected on profiles of thickness ratios of the order of 10 percent. The flow separation can cause negative lift coefficients, control surface oscillation, and rapid changes in the location of the center of lift.

5. The location of the center of lift is greatly influenced by flow separation and the movement of shock waves over the airfoil surface at high subsonic speeds. Each particular profile presents different problems depending on the airfoil thickness ratio and the proportion of subsonic to supersonic flow over the airfoil surface.

6. The transonic similarity rules advocated by Spreiter are applicable at subsonic speeds when his assumptions, $\alpha \ll t/c$ and $C_L \sim \alpha$, are not violated, and when boundary layer effects are small.

7. The experimental results for the lift of wedges are in agreement with the computations of Guderley and Yoshihara for Mach number one.

APPENDIX A

AIRFOIL CHARACTERISTICS NEAR MACH NUMBER ONE

Previously, Liepmann and Bryson (Ref. 11) have proposed that for steady flow near $M_\infty = 1$, the local Mach number at any point on a body does not change with changes in free stream Mach number. They expressed this by setting

$$\left[\frac{\partial M}{\partial M_\infty} \right]_{M_\infty = 1} = 0 \quad (\text{A-1})$$

Bryson (Ref. 1) then used the exact pressure coefficient formula

$$C_p = \frac{2}{\gamma M_\infty^2} \left[\left(\frac{1 + \frac{\gamma-1}{2} M_\infty^2}{1 + \frac{\gamma-1}{2} M^2} \right)^{\gamma/(\gamma-1)} - 1 \right] \quad (\text{A-2})$$

and Eq. (A-1) to compute the slope of the drag coefficient at Mach number one.

Here, using a method suggested by Drougge (Ref. 25), the drag curve itself can be computed for M_∞ near one.

For a two-dimensional body the drag coefficient is

$$C_D = -\frac{1}{C} \oint C_p (\bar{i} \cdot \bar{n}) ds \quad (\text{A-3})$$

where

\bar{i} = unit vector in stream direction

\bar{n} = unit vector normal to profile pointing outward

ds = element of length along profile contour

Using Eq. (A-2)

$$C_D = -\frac{1}{C} \frac{2}{\gamma M_\infty^2} \left[\left(1 + \frac{\gamma-1}{2} M_\infty^2 \right)^{\gamma/(\gamma-1)} \oint \frac{\bar{i} \cdot \bar{n} ds}{\left(1 + \frac{\gamma-1}{2} M^2 \right)^{\gamma/(\gamma-1)}} - \oint (\bar{i} \cdot \bar{n}) ds \right] \quad (\text{A-4})$$

But, according to the stationarity principle, M is not a function of M_∞ near $M_\infty = 1$. Thus, the first integral of (A-4) is a constant near $M_\infty = 1$ and the second is zero. Therefore, including $-1/c$ in the constant, Eq. (A-4) becomes

$$C_D = \frac{2}{\gamma M_\infty^2} \left(1 + \frac{\gamma-1}{2} M_\infty^2 \right)^{\gamma/\gamma-1} \text{CONST.} \quad (\text{A-5})$$

But at $M_\infty = 1$, $C_D = C_D^*$ so the constant may be evaluated, giving the result

$$\frac{C_D}{C_D^*} = \frac{1}{M_\infty^2} \left[\frac{2 + (\gamma-1) M_\infty^2}{\gamma+1} \right]^{\gamma/\gamma-1} \quad (\text{A-6})$$

if the relation

$$M^2 = \frac{2}{\frac{\gamma+1}{M^{*2}} - (\gamma-1)} \quad (\text{A-7})$$

between M and M^* is substituted into (A-6) and M^* is approximated by $M^* \doteq 1 + \epsilon$ for $\epsilon \ll 1$. The result is, to the first order,

$$\frac{C_D}{C_D^*} = \frac{1}{M^*} \quad (\text{A-8})$$

which is Drougge's result (Ref. 25).

The same process may be carried out for the lift coefficient of a two-dimensional body at constant angle of attack when M_∞ is near one. Here,

$$C_L = -\frac{1}{c} \oint C_p (\bar{j} \cdot \bar{n}) ds \quad (\text{A-9})$$

where

\bar{j} = unit vector normal to stream direction

This is similar to Eq. (A-3) and following the same procedure as before one obtains

$$\frac{C_L}{C_L^*} = \frac{1}{M_\infty^2} \left[\frac{2 + (\gamma-1) M_\infty^2}{\gamma+1} \right]^{\gamma/\gamma-1}, \quad \alpha = \text{CONST.} \quad (\text{A-10})$$

or, to the first order,

$$\frac{C_L}{C_L^*} = \frac{1}{M^*}, \quad \alpha = \text{CONST.} \quad (\text{A-11})$$

If it is assumed that lift is a linear function of angle of attack for $\alpha \ll 1$, then

$$\frac{\partial C_L}{\partial \alpha} = \frac{C_L}{\alpha} \quad (\text{A-12})$$

and the result for the lift curve slope near $M_\infty = 1$ is

$$\frac{C_L/\alpha}{(C_L/\alpha)^*} = \frac{1}{M_\infty^2} \left[\frac{2 + (\gamma-1) M_\infty^2}{\gamma+1} \right]^{\gamma/\gamma-1} \quad (\text{A-13})$$

In addition, the moment coefficient about the leading edge is

$$C_m = \frac{1}{C^2} \oint x C_p (\bar{j} \cdot \bar{n}) ds \quad (\text{A-14})$$

Thus, for constant α , near $M_\infty = 1$

$$\frac{C_m}{C_m^*} = \frac{1}{M_\infty^2} \left[\frac{2 + (\gamma-1) M_\infty^2}{\gamma+1} \right]^{\gamma/\gamma-1} \quad (\text{A-15})$$

Eq. (A-15) was derived in the same way as Eq. (A-4), using the fact that

$$\oint x (\bar{j} \cdot \bar{n}) ds = 0 \quad (\text{A-16})$$

If the moment coefficient is linear in angle of attack for $\alpha \ll 1$, a result for $\partial C_m / \partial \alpha$ similar to that for $\partial C_L / \partial \alpha$ is obtained. All the previous results may be collected here

$$\frac{C_D}{C_D^*} = \frac{C_L}{C_L^*} = \frac{C_m}{C_m^*} = \frac{C_L/\alpha}{(C_L/\alpha)^*} = \frac{C_m/\alpha}{(C_m/\alpha)^*} = \frac{1}{M_\infty^2} \left[\frac{2 + (\gamma-1) M_\infty^2}{\gamma+1} \right]^{\gamma/\gamma-1} \approx \frac{1}{M^*}$$

From the definition of the location of center of lift from the leading edge

$$\frac{x}{c} = - \frac{C_m}{C_L} \quad (\text{A-18})$$

and Eq. (A-17), it follows that

$$\frac{x}{c} = \left(\frac{x}{c} \right)^* \quad (\text{A-19})$$

for M_∞ near one.

Eq. (A-17) can be differentiated with respect to M_∞ and M_∞ set equal to one to obtain

$$\begin{aligned} \frac{1}{C_D^*} \left(\frac{dC_D}{dM_\infty} \right)^* &= \frac{1}{C_L^*} \left(\frac{dC_L}{dM_\infty} \right)^* = \frac{1}{C_m^*} \left(\frac{dC_m}{dM_\infty} \right)^* = \frac{1}{(C_L/\alpha)^*} \left(\frac{d(C_L/\alpha)}{dM_\infty} \right)^* \\ &= \frac{1}{(C_m/\alpha)^*} \left(\frac{d(C_m/\alpha)}{dM_\infty} \right)^* = - \frac{2}{\gamma+1} \end{aligned} \quad (\text{A-20})$$

which corresponds to Bryson's result (Ref. 1) for the slope of the air-foil drag coefficient only at $M_\infty = 1$.

The results of Eq. (A-20) and not Eq. (A-17) were used on the plots of Figs. 22 and 23, due to the lack of experimental data near $M_\infty = 1$.

APPENDIX B
THE MEASUREMENT OF SURFACE PRESSURE
WITH STATIC PROBES

Surface pressures on two-dimensional bodies of small thickness ratio can be measured by traversing a conventional static pressure probe over the surface. The method can be applied to thin bodies which are difficult, if not impossible, to instrument with conventional surface pressure taps. The same method should prove very useful in problems involving the shaping of aerodynamic surfaces to obtain a given pressure distribution, for example, in wind tunnel tests on pylons, fuselage-wing fillets, etc.

The fact that surface pressures on thin bodies can be measured with precision at points off the surface depends on two effects. The first is the effect of viscosity in providing a boundary layer through which the static pressure is constant in a direction normal to the body surface when the surface curvature is small. The second effect depends on the fluid being irrotational outside of the boundary layer. In conventional notation, using two-dimensional perturbation velocities, u and v , the irrotationality condition is

$$u_y - v_x = 0 \quad (B-1)$$

The linearized boundary condition on the body surface is

$$v/U_\infty \doteq (\text{body slope}) \quad \text{on } y = 0 \quad (B-2)$$

and the pressure coefficient is

$$C_p \doteq - (2u/U_\infty) \quad (B-3)$$

From Eqs. (B-1) and (B-2), it is apparent that in the inviscid

flow near the surface the change in u in the y -direction is proportional to the x -derivative of the slope of the body when the boundary layer growth is small. For flat surfaces $\partial u / \partial y$ is negligible and from Eq. (B-3) the pressure change normal to the surface ($y = 0$) will be very small. On slightly curved surfaces the change of body slope is small and the normal pressure gradients must also be small.

Using the above considerations, a pair of slender static pressure probes were used to measure the pressure distribution on an airfoil. The probe arrangement on the airfoil cross section is shown in Fig. 2. In order to minimize tunnel blockage, the probes slide inside larger supporting tubes which lead back from the airfoil and out through the tunnel wall. The probes were held together by a loop of wire approximately two diameters from the tips. The wire loop also made the probe boundary layer turbulent, which is important when measuring steep pressure gradients (Ref. 22). The ratio of probe diameter to airfoil thickness was of the order of one-half.

The effect of the small three-dimensional probe disturbances on the basic two-dimensional flow over the airfoil was checked with the Mach-Zehnder interferometer, described in Ref. (16). An interferogram of the flow over one surface of the 3 percent thick airfoil shown in Fig. 2 was made and the pressure distribution computed. The probes were then installed and used to find the surface pressure distribution. The airfoil was investigated for an angle of attack of approximately one degree at two supersonic Mach numbers. On one case the bow shock wave was attached with completely supersonic flow over the airfoil. The second case was at a lower Mach number with a detached bow wave

giving subsonic flow over the front portion of the airfoil. The agreement between interferometer and probe measurements was good except in the vicinity of the airfoil nose, as shown in Fig. 3.

APPENDIX C

COMPUTATION OF THE LIFT OF A TRUNCATED WEDGE

An approximate computation for the lift of a truncated wedge at high subsonic speeds and small angle of attack will be discussed. This computation is based on the transonic approximation to the equations of gas dynamics (Ref. 4) and depends on the previous work of Cole (Ref. 20). The method was suggested by the work of Guderley and Yoshihara (Ref. 8) who computed the lift of a double wedge at sonic speed using the assumption that for small angles the change in pressure is proportional to the angle of attack. The present method of solution differs from that of Guderley and Yoshihara in that the free stream singularity is not shifted, but it is essentially the same as that used by Vincenti and Wagoner (Ref. 9) in their independent computation of the subsonic flow field at an angle of attack over the front portion of a double wedge with a detached bow wave. The author wishes to thank Dr. J. D. Cole for his suggestions and useful criticism.

1. Equations of Motion

The equations of motion are the two-dimensional equations of gas dynamics which are approximately valid for the transonic flow of a non-viscous, compressible fluid. A discussion of the equations and their applicability has been given by Spreiter (Ref. 6), who showed that the transonic equations are valid throughout the subsonic and low supersonic Mach number range.

In the hodograph plane the equations of continuity and

irrotationality are given approximately by:

$$u y_v - x_u = 0 \quad (C-1)$$

$$x_v - y_u = 0 \quad (C-2)$$

The notation of Ref. (20) will be used throughout this appendix. Substitution of $-w$ for u and elimination of x yields

$$w y_{vv} + y_{ww} = 0 \quad (C-3)$$

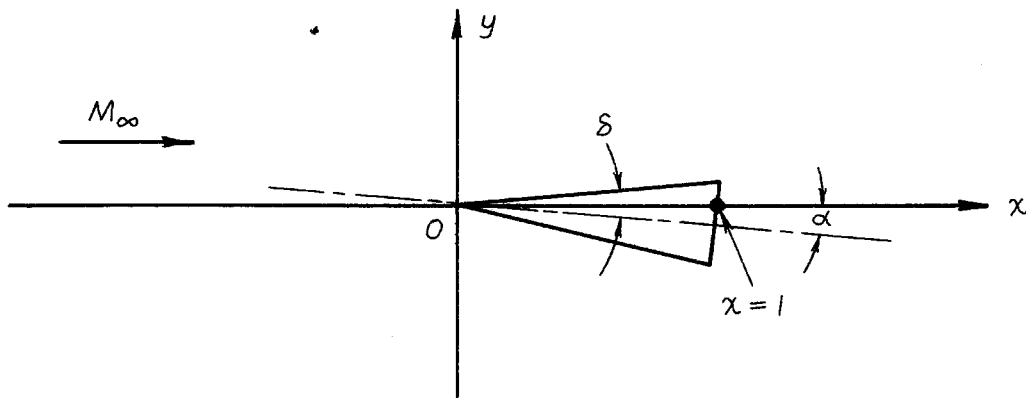
an equation of mixed type studied by Tricomi (Ref. 26). Eq. (C-3) will be approximately solved for the lifting finite wedge and the pressure forces on the wedge surface obtained from this solution with the aid of Eq. (C-2) and the formula for the local pressure coefficient

$$C_p = \frac{2}{\gamma+1} (w - w_i) = \frac{2}{\gamma+1} \left(\frac{3}{2} \right)^{2/3} \left[Z^{2/3} - Z_i^{2/3} \right] \quad (C-4)$$

where the substitution $Z = (2/3) w^{3/2}$ has been made.

2. Formulation of the Boundary Value Problem

The wedge has a semi-angle δ and the axis of symmetry of the wedge cross section is inclined at an angle α to the uniform subsonic flow at upstream infinity (Sketch C-1).



Sketch C-1

The angle α is assumed to be much less than δ . The nose of the wedge is located at the origin of the coordinate system, and the wedge has unit length. Since the Mach number of the flow is given approximately by

$$1 - M^2 = w \quad (C-5)$$

The uniform perturbation velocity at infinity is

$$w_1 = 1 - M_\infty^2 = \left(\frac{3}{2} z_1 \right)^{2/3} \quad v = 0 \quad (C-6)$$

Another condition is that the flow must be tangent to the body surface.

The actual condition is $\frac{v}{\gamma + 1 + w} = \tan(\delta - \alpha)$ on the upper surface and $\frac{v}{\gamma + 1 + w} = \tan(-\delta - \alpha)$ on the lower surface. These are approximated by

$$\begin{aligned} v &= (\gamma + 1)(\delta - \alpha) = v_0 - \epsilon \quad \text{for} \quad y = 0^+, \quad 0 < x < 1 \\ v &= -(\gamma + 1)(\delta + \alpha) = -v_0 - \epsilon \quad \text{for} \quad y = 0^-, \quad 0 < x < 1 \end{aligned} \quad (C-7)$$

where $v_0 = (\gamma + 1)\delta$ and $\epsilon = (\gamma + 1)\alpha$. In addition, it can be shown (Ref. 29) that sonic velocity must be reached at the wedge shoulders. Sonic velocity will also be obtained as the flow expands over the upper side of the wedge nose, but Guderley and Yoshihara have shown (Ref. 8) that at $M_\infty = 1$, for vanishingly small angles of attack, the nose expansion effect can be neglected. Thus, in the neighborhood of the nose, assuming the result of Ref. (8) to be valid for $M_\infty < 1$, the principal effect is a stagnation point which may be approximated by the stagnation condition of linearized theory.

$$w \rightarrow \infty \quad \text{at} \quad x = 0, \quad y = 0 \quad (C-8)$$

The boundary value problem in the hodograph plane can now be formulated. The problem will be approximately solved by assuming

$$y(w, v) = y_0(w, v) + \epsilon y_1(w, v) \quad (C-9)$$

and

$$\chi(w, v) = \chi_0(w, v) + \epsilon \chi_1(w, v) \quad (C-10)$$

where χ_0 and y_0 refer to the solution of Cole (Ref. 20) for a finite wedge at zero angle of attack. Hence, the first order perturbation solution for the wedge at an angle of attack is given by y_1 and χ_1 .

The boundary conditions for χ and y in the hodograph plane are obtained from the previous physical plane conditions. At infinity condition (C-6) becomes

$$y \rightarrow \pm \infty, \quad \chi \rightarrow \pm \infty \quad \text{when} \quad w = w_1, \quad v = 0 \quad (C-11)$$

which represents the free stream singularity and is discussed in Ref. (20). On the wedge surfaces

$$\begin{aligned} y = 0 \quad \text{on} \quad v = v_0 - \epsilon \\ y = 0 \quad \text{on} \quad v = -v_0 - \epsilon \end{aligned} \quad (C-12)$$

and at the linearized nose stagnation point

$$y = 0, \quad \chi = 0 \quad \text{as} \quad w \rightarrow \infty \quad (C-13)$$

Also, the attainment of sonic velocity at the shoulder determines the wedge length in the hodograph. The exact condition is that on the upper or lower surface χ equals one plus or minus a small quantity accounting for the change in the χ coordinate of the shoulder as the wedge is rotated through an angle α . For small α this correction term is approximately equal to $\pm \alpha \delta$. The correction term will be ignored, and the problem solved will be that for a slightly deformed wedge whose shoulders remain at $\chi = 1$ as α is changed. Hence, the wedge length in the hodograph is given approximately by

$$\chi = 1 \quad \text{when} \quad w = 0, \quad v = \pm v_0 - \epsilon \quad (C-14)$$

Finally, if the expansion of the flow over the nose of the wedge is ignored, all subsonic points of the physical plane, including the sonic line, are mapped into a semi-infinite strip with

$$-v_0 - \epsilon \leq v \leq v_0 - \epsilon, \quad w > 0 \quad (C-15)$$

as discussed in Ref. (20).

The conditions on the wedge surface (C-12) may be expanded in a Taylor series about $v = \pm v_0$:

$$\begin{aligned} 0 &= y(w, v_0) - \epsilon y_v(w, v_0) + \theta(\epsilon^2) & \text{for } v = v_0 - \epsilon \\ 0 &= y(w, -v_0) - \epsilon y_v(w, -v_0) + \theta(\epsilon^2) & \text{for } v = -v_0 - \epsilon \end{aligned} \quad (C-16)$$

These become

$$\begin{aligned} 0 &= y_0(w, v_0) + \epsilon [y_1(w, v_0) - y_{0v}(w, v_0)] + \theta(\epsilon^2) & \text{for } v = v_0 - \epsilon \\ 0 &= y_0(w, -v_0) + \epsilon [y_1(w, -v_0) - y_{0v}(w, -v_0)] + \theta(\epsilon^2) & \text{for } v = -v_0 - \epsilon \end{aligned} \quad (C-17)$$

when substitution of Eq. (C-9) is made. Cole's solution for $y_0(w, v)$ and $x_0(w, v)$ of Ref. (20) satisfies the following conditions

$$\begin{aligned} y_0 &= 0 & \text{at } v = \pm v_0 \\ y_0 &= 0, \quad x_0 = 0 & \text{as } w \rightarrow \infty \\ x_0 &= 1 & \text{at } v = \pm v_0, \quad w = 0 \end{aligned} \quad (C-18)$$

Thus, the conditions (C-13), (C-14), and (C-17) which y_1 and x_1 must satisfy are:

$$y_1 = 0, \quad x_1 = 0 \quad \text{as } w \rightarrow \infty \quad (C-19)$$

$$x_1 = 0 \quad \text{at } v = \pm v_0, \quad w = 0 \quad (C-20)$$

$$y_1 = y_{0v} = f(z) \quad \text{at } v = \pm v_0 \quad (C-21)$$

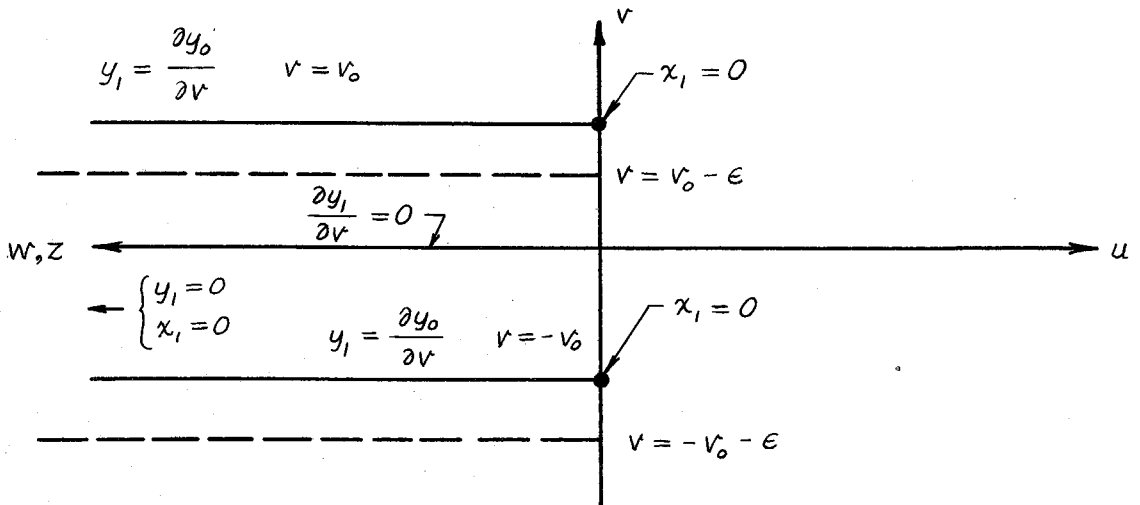
It will be noted that the above conditions for y_1 and x_1 are satisfied on the symmetric hodograph boundaries for a wedge at zero angle of

attack instead of on the actual unsymmetric boundaries.

The solution for y_1 may be simplified by symmetry considerations. It can be shown that y_1 is an even function of v by the following argument. If the wedge is at a positive angle of attack $\alpha = \alpha'$, then at a point x', y' let the perturbation velocity in the x direction be denoted by w' and the vertical velocity by v' . If the wedge is now rotated to a negative angle of attack $\alpha = -\alpha'$, the perturbation velocities at the point $x', -y'$ must be w' and $-v'$ by symmetry. From Eq. (C-9) and the fact that $y_0(w', v') = -y_0(w', -v')$ it is apparent that $y_1(w', v') = y_1(w', -v')$. Thus, $y_1(w, v)$ is an even function of v . Hence from Eq. (C-2) it is apparent that $x_1(w, v) = -x_1(w, -v)$ and $x_1(w, v)$ is an odd function of v . The solution for y_1 and x_1 may now be obtained in the upper half of the strip $0 \leq v \leq v_0$, $w > 0$ if the symmetry of y_1 is expressed by the boundary condition

$$\frac{\partial y_1}{\partial v} = 0 \quad \text{at} \quad v = 0, \quad w > 0 \quad (\text{C-22})$$

The conditions (C-19) through (C-22) are shown in Sketch C-2, where



Sketch C-2

the dashed lines of constant ψ indicate the actual boundaries for a wedge at angle of attack.

3. Representation of the Solution

A solution of Eq. (C-3) obtained by separation of variables is

$$y_1 \sim e^{\pm \lambda v} z^{1/3} C_{1/3}(\lambda z) \quad (C-23)$$

Using solutions of this type a solution for y_1 which satisfies Eq. (C-22) is

$$y_1 = z^{1/3} \int_0^\infty \frac{\cosh \lambda v}{\cosh \lambda v_0} J_{-1/3}(\lambda z) \lambda d\lambda \int_0^\infty f(z') J_{-1/3}(\lambda z') z' dz' \quad (C-24)$$

Here $J_{-1/3}$ is used instead of $J_{+1/3}$, since $J_{+1/3}$ has $y_1 = \frac{\partial y_1}{\partial v} = 0$ on the sonic line, $z = 0$. Thus, the flow field on the sonic line would not change when the angle of attack changed, if $J_{+1/3}$ were used.

At $v = v_0$

$$y_1(z, v_0) = z^{1/3} \int_0^\infty J_{-1/3}(\lambda z) \lambda d\lambda \int_0^\infty f(z') J_{-1/3}(\lambda z') z' dz' \quad (C-25)$$

using Hankel's repeated integral formula (Ref. 27)

$$\int_0^\infty z' dz' \int_0^\infty F(\sigma) J_{\nu}(z'\sigma) J_{\nu}(z'\lambda) \sigma d\sigma = F(\lambda) \quad (C-26)$$

Eq. (C-25) becomes

$$y_1(z, v_0) = z^{1/3} f(z) \quad (C-27)$$

In order to satisfy Eq. (C-21)

$$f(z) = \frac{y_{0v}(z, v_0)}{z^{1/3}} \quad (C-28)$$

From Ref. (20)

$$f(z) = \frac{y_{0v}(z, v_0)}{z^{1/3}} = - \left(\frac{2z_1}{3} \right)^{1/3} v_0 \int_0^\infty \frac{J_{-1/3}(\sigma z') J_{-1/3}(\sigma z_1) \sigma^2 d\sigma}{\sinh \sigma v_0} \quad (C-29)$$

Thus Eq. (C-24) becomes

$$y_1(z, v) = - \left(\frac{2zz_1}{3} \right)^{1/3} v_0 \int_0^\infty \frac{\cosh \lambda v}{\cosh \lambda v_0} J_{-1/3}(\lambda z) \lambda d\lambda \int_0^\infty J_{-1/3}(\lambda z') z' dz' \int_0^\infty \frac{J_{-1/3}(\sigma z') J_{-1/3}(\sigma z_1) \sigma^2 d\sigma}{\sinh \sigma v_0} \quad (C-30)$$

which becomes with the use of Eq. (C-26)

$$y_1(z, v) = - \left(\frac{2zz_1}{3} \right)^{1/3} v_0 \int_0^\infty \frac{\cosh \lambda v}{\cosh \lambda v_0 \sinh \lambda v_0} J_{-1/3}(\lambda z) J_{-1/3}(\lambda z_1) \lambda^2 d\lambda \quad (C-31)$$

It may also be seen from the asymptotic behavior of $J_{1/2}$

$$J_{1/2}(z) \cong \sqrt{\frac{2}{\pi z}} \cos \left(z - \frac{3\pi}{2} - \frac{\pi}{4} \right) \quad (C-32)$$

that $y_1(z, v)$ of Eq. (C-31) approaches zero as $z \rightarrow \infty$ so that

Eq. (C-19) is satisfied.

From Eq. (C-2)

$$x_v = y_u = -y_w = -\sqrt{w} \quad y_z = - \left(\frac{3z}{2} \right)^{1/3} y_z \quad (C-33)$$

so that the value of $x_1(z, v)$ corresponding to Eq. (C-31) may be obtained. Using

$$\frac{\partial}{\partial z} \left[z^{1/3} J_{-1/3}(\lambda z) \right] = -\lambda z^{1/3} J_{2/3}(\lambda z) \quad (C-34)$$

we have

$$x_{1v} = - (z^2 z_1)^{1/3} v_0 \int_0^\infty \frac{\cosh \lambda v}{\cosh \lambda v_0 \sinh \lambda v_0} J_{2/3}(\lambda z) J_{-1/3}(\lambda z_1) \lambda^3 d\lambda \quad (C-35)$$

Integrating with respect to v

$$x_1 = - (z^2 z_1)^{1/3} v_0 \int_0^\infty \frac{\sinh \lambda v}{\cosh \lambda v_0 \sinh \lambda v_0} J_{2/3}(\lambda z) J_{-1/3}(\lambda z_1) \lambda^2 d\lambda + x_2(z) \quad (C-36)$$

Considering Eq. (C-1) it can be shown that χ_2 must be constant. From condition (C-20) and the fact that the series for $J_{2/3}(\lambda z)$ contains only positive powers of λz it is apparent that $\chi_2 = 0$. Collecting the results, the integral representation for y_1 and χ_1 is

$$y_1(z, v) = -\left(\frac{2zz_1}{3}\right)^{1/3} v_0 \int_0^\infty \frac{\cosh \lambda v}{\cosh \lambda v_0 \sinh \lambda v_0} J_{-1/3}(\lambda z) J_{-1/3}(\lambda z_1) \lambda^2 d\lambda \quad (C-39)$$

$$\chi_1(z, v) = -(z^2 z_1)^{1/3} v_0 \int_0^\infty \frac{\sinh \lambda v}{\cosh \lambda v_0 \sinh \lambda v_0} J_{2/3}(\lambda z) J_{-1/3}(\lambda z_1) \lambda^2 d\lambda \quad (C-40)$$

The solution given by Eqs. (C-39) and (C-40) will now be discussed. From Ref. (20), the solution for y_0 and χ_0 has a doublet singularity representing the free stream. The sonic line is straight in the physical plane, so that y_0 and χ_0 satisfy the problem for a finite wedge of unit length at zero angle of attack, with sonic lines located at $\chi = 1$. The additional solutions χ_1 and y_1 are non-singular and the sonic line is still located at $\chi = 1$. The solutions χ_1 and y_1 do fulfill, to the first order in α , the condition that the flow be tangent to the surface of the wedge. It will be noted that no attempt has been made either in Ref. (20) or here to account for the influence on the upstream subsonic flow of the supersonic flow around the wedge shoulders. This has already been discussed in Section IV.

4. Lift Coefficient of the Wedge

The lift coefficient is defined as

$$C_L = \frac{\text{LIFT FORCE}}{\frac{1}{2} \rho_\infty (a^* + u_\infty)^2} \quad \text{PER UNIT WIDTH} \quad (C-41)$$

Using the local pressure coefficient of Eq. (C-4) the lift coefficient becomes

$$C_L = \int_0^1 (C_{p_L} - C_{p_U}) dx = \frac{2}{\gamma+1} \left(\frac{3}{2}\right)^{2/3} \int_0^1 (z_L^{2/3} - z_U^{2/3}) dx \quad (C-42)$$

where the subscripts L and U refer to the lower and upper surfaces.

Since $x = x(z)$ on the wedge surface, C_L becomes

$$C_L = \frac{2}{\gamma+1} \left(\frac{3}{2}\right)^{2/3} \int_0^\infty z^{2/3} \left[\left(\frac{\partial x}{\partial z}\right)_U - \left(\frac{\partial x}{\partial z}\right)_L \right] dz \quad (C-43)$$

Using the formula for x , Eq. (C-10), and the symmetry conditions

$(x_0)_L = (x_0)_U$ and $(x_1)_L = -(x_1)_U$, Eq. (C-43) becomes

$$C_L = 4\alpha \left(\frac{3}{2}\right)^{2/3} \int_0^\infty z^{2/3} \left(\frac{\partial x_1}{\partial z}\right)_U dz \quad (C-44)$$

Integrating by parts and using conditions (C-19) and (C-20) on x_1 , we have

$$C_L = -4\alpha \left(\frac{2}{3}\right)^{1/3} \int_0^\infty z^{-1/3} x_1(z) dz \quad (C-45)$$

Upon substituting Eq. (C-40) into Eq. (C-45) and integrating with respect to z ,

$$\frac{C_L}{\alpha} = \left(\frac{4}{3}\right)^{1/3} \frac{4}{\Gamma\left(\frac{2}{3}\right)} v_o z_1^{1/3} \int_0^\infty \frac{J_{-1/3}(\lambda z_1) \lambda^{2/3} d\lambda}{\cosh \lambda v_o} \quad (C-46)$$

Or using the similarity parameters

$$\tilde{C}_L = v_o^{1/3} C_L = [(\gamma+1) \delta]^{1/3} C_L ; \quad \xi_\infty = -\left(\frac{3}{2} \frac{z_1}{v_o}\right)^{2/3} = \frac{M_\infty^2 - 1}{[(\gamma+1) \delta]^{2/3}}$$

Eq. (C-46) becomes

$$\frac{\tilde{C}_L}{\alpha} = -\left(\frac{8}{9}\right)^{1/3} \frac{4 \xi_\infty^{1/2}}{\Gamma\left(\frac{2}{3}\right)} \int_0^\infty \frac{J_{-1/3}\left(\frac{-2\sigma}{3} \xi_\infty^{3/2}\right)}{\cosh \sigma} \sigma^{2/3} d\sigma \quad (C-47)$$

Using a partial fraction expansion for $1/\cosh \sigma$ (Ref. 28),

$$\frac{\tilde{C}_L}{\alpha} = -\left(\frac{8}{9}\right)^{1/3} \frac{8\xi_\infty^{1/2}}{\Gamma\left(\frac{2}{3}\right)} \sum_{m=0}^{\infty} (-1)^m \left(m + \frac{1}{2}\right) \pi \int_0^{\infty} \frac{J_{-1/3}\left(\frac{-2\sigma}{3} \xi_\infty^{3/2}\right) \sigma^{2/3} d\sigma}{\left(m + \frac{1}{2}\right)^2 \pi^2 + \sigma^2} \quad (C-48)$$

The integral is evaluated in Ref. 27, p. 424. Therefore

$$\frac{\tilde{C}_L}{\alpha} = -\left(\frac{8}{9}\right)^{1/3} \frac{8\xi_\infty^{1/2}}{\Gamma\left(\frac{2}{3}\right)} \sum_{m=0}^{\infty} (-1)^m \left(m + \frac{1}{2}\right)^{2/3} \pi^{2/3} K_{+1/3} \left[-\frac{2\pi}{3} \left(m + \frac{1}{2}\right) \xi_\infty^{3/2} \right] \quad (C-49)$$

The series converges rapidly for large values of the argument of $K_{+1/3}$, however, for small values of the argument the convergence is slow. If the expansion for $1/\cosh \sigma$ is taken to be

$$\frac{1}{\cosh \sigma} = 2 \sum_{m=0}^{\infty} (-1)^m e^{-(2m+1)\sigma}$$

then the integral occurring in Eq. (C-48) is different and has also been evaluated in Ref. 27, p. 386. Therefore, for small arguments

$$\frac{\tilde{C}_L}{\alpha} = \frac{16}{3^{1/3}} \frac{\Gamma\left(\frac{4}{3}\right)}{\left[\Gamma\left(\frac{2}{3}\right)\right]^2} \sum_{m=0}^{\infty} (-1)^m \frac{(2m+1)}{\left[(2m+1)^2 - \left(\frac{2}{3}\right)^2 \xi_\infty^3\right]^{7/6}} \quad (C-50)$$

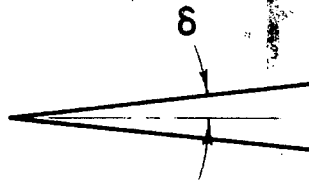
Using Eqs. (C-49) and (C-50) the curve shown on Fig. 7 has been computed. The results have been discussed in Section IV. In particular at $M_\infty = 1$, $\tilde{C}_L/\alpha \doteq 4.54$ which is approximately 10 percent lower than Guderley and Yoshihara's result for the lift of the front half of a double wedge.

REFERENCES

1. Bryson, A. E. Jr.: An Experimental Investigation of Transonic Flow Past Two-Dimensional Wedge and Circular-Arc Sections Using a Mach-Zehnder Interferometer. NACA TR 1094, 1952; supercedes NACA TN 2560, 1951.
2. Solomon, G. E.: Transonic Flow Past Cone-Cylinders. Thesis, California Institute of Technology, 1953.
3. Goethert, B.: Airfoil Measurements in the D.V.L. High-Speed Wind Tunnel. NACA TM 1240, 1949. Translation of "Profilmessungen im D.V.L. Hochgeschwindigkeitswindkanal." Lilienthal-Gesellschaft für Luftfahrtforschung, Bericht 156, 1942.
4. von Kármán, T.: The Similarity Law of Transonic Flow. Jour. Math. and Phys., Vol. XXVI, 1947.
5. Busemann, A.: Application of Transonic Similarity. NACA TN 2687, 1952.
6. Spreiter, J. R.: On the Application of Transonic Similarity Rules. NACA TN 2726, 1952.
7. Harder, K. C.: Transonic Similarity Rules for Lifting Wings. NACA TN 2724, 1952.
8. Guderley, G. and Yoshihara, H.: Two-Dimensional Unsymmetric Flow Patterns at Mach Number One. Air Force Technical Report 6683, 1952.
9. Vincenti, W. G. and Wagoner, C. B.: Theoretical Study of the Lift of a Double Wedge Profile with Detached Bow Wave. NACA TN 2832, 1952.
10. Gullstrand, T. R.: The Flow Over Two-Dimensional Aerofoils at Incidence in the Transonic Speed Range. Royal Institute of Technology, Division of Aeronautics, K.T.H. Aero. TN 27, 1952.
11. Liepmann, H. W. and Bryson, A. E. Jr.: Transonic Flow Past Wedge Sections. Jour. Aero. Sciences, Vol. 17, 1950.
12. Guderley, G.: Considerations of the Structure of Mixed Subsonic-Supersonic Flow Patterns. U.S. Air Force Report, F-TR-2168-ND, 1947.
13. Guderley, G. and Yoshihara, H.: The Flow Over a Wedge Profile at Mach Number One. Jour. Aero. Sciences, Vol. 18, 1951.

14. Vincenti, W. G. and Wagoner, C. B.: Transonic Flow Past a Wedge Profile with Detached Bow Wave--General Analytical Method and Final Calculated Results. NACA TN 2339, 1951.
15. Griffith, W.: Shock-Tube Studies of Transonic Flow Over Wedge Profiles. Jour. Aero. Sciences, Vol. 19, 1952.
16. Ashkenas, H. T. and Bryson, A. E.: Design and Performance of a Simple Interferometer for Wind-Tunnel Measurements. Jour. Aero. Sciences, Vol. 18, 1951.
17. Dhawan, S. and Roshko, A.: A Flexible Nozzle for a Small Supersonic Wind Tunnel. Jour. Aero. Sciences, Vol. 18, 1951.
18. Eggers, A. J.: Aerodynamic Characteristics at Subcritical and Supercritical Mach Numbers of Two Airfoils Having Sharp Leading Edges and Extreme Rearward Positions of Maximum Thickness. NACA RM A7C10, 1947.
19. Tsien, H. S. and Lees, L.: The Glauert-Prandtl Approximation for Subsonic Flows of a Compressible Fluid. Jour. Aero. Sciences, Vol. 12, 1945.
20. Cole, J. D.: Drag of a Finite Wedge at High Subsonic Speeds. Jour. Math. and Phys., Vol. XXX, 1951.
21. Bartlett, G. E. and Peterson, J. W.: Wind Tunnel Investigation of a Double Wedge Airfoil at High Subsonic Speeds. Cornell Aero. Lab., Report AF-360-A-6, 1946.
22. Liepmann, H. W., Roshko, A. and Dhawan, S.: On Reflection of Shock Waves From Boundary Layers. NACA TN 2334, 1951.
23. Goethert, B. Ruderwirkung bei hohen Unterschallgeschwindigkeiten. Lilienthal-Gesellschaft für Luftfahrtforschung, Bericht 156, 1942.
24. Ackeret, J.: Experiments on Airfoils with Trailing Edge Cut Away. NACA TM 431, 1927.
25. Drougge, G.: Note on Wall Interference in Two-Dimensional Flow at Subsonic and Transonic Speeds. The Aeronautical Research Institute of Sweden, Report 40, 1951.
26. Tricomi, F.: On Linear Partial Differential Equations of Mixed Type. Brown Univ. translation A9-T-26 of article in Atti. della R. Acc. Naz. dei Lincei, Serie Quinta, Memorie etc., 14, 1923.
27. Watson, G. N.: A Treatise on the Theory of Bessel Functions. Cambridge Univ. Press, 1948.
28. Whittaker, E. T. and Watson, G. N.: A Course of Modern Analysis. Cambridge Univ. Press, 1947.

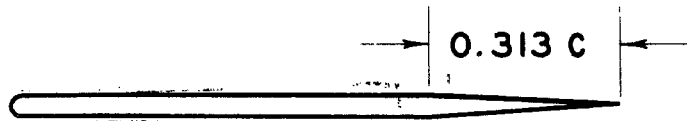
29. Cole, J. D.: Problems in Transonic Flow. Thesis, Calif. Institute of Technology, 1949.



TRUNCATED WEDGE

$C = 1''$

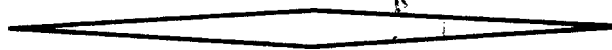
$\delta = 5.97^\circ$



ROUND NOSE AIRFOIL

$C = 2''$

$t/c = .033$



DOUBLE WEDGE

$C = 2''$

$t/c = .054$



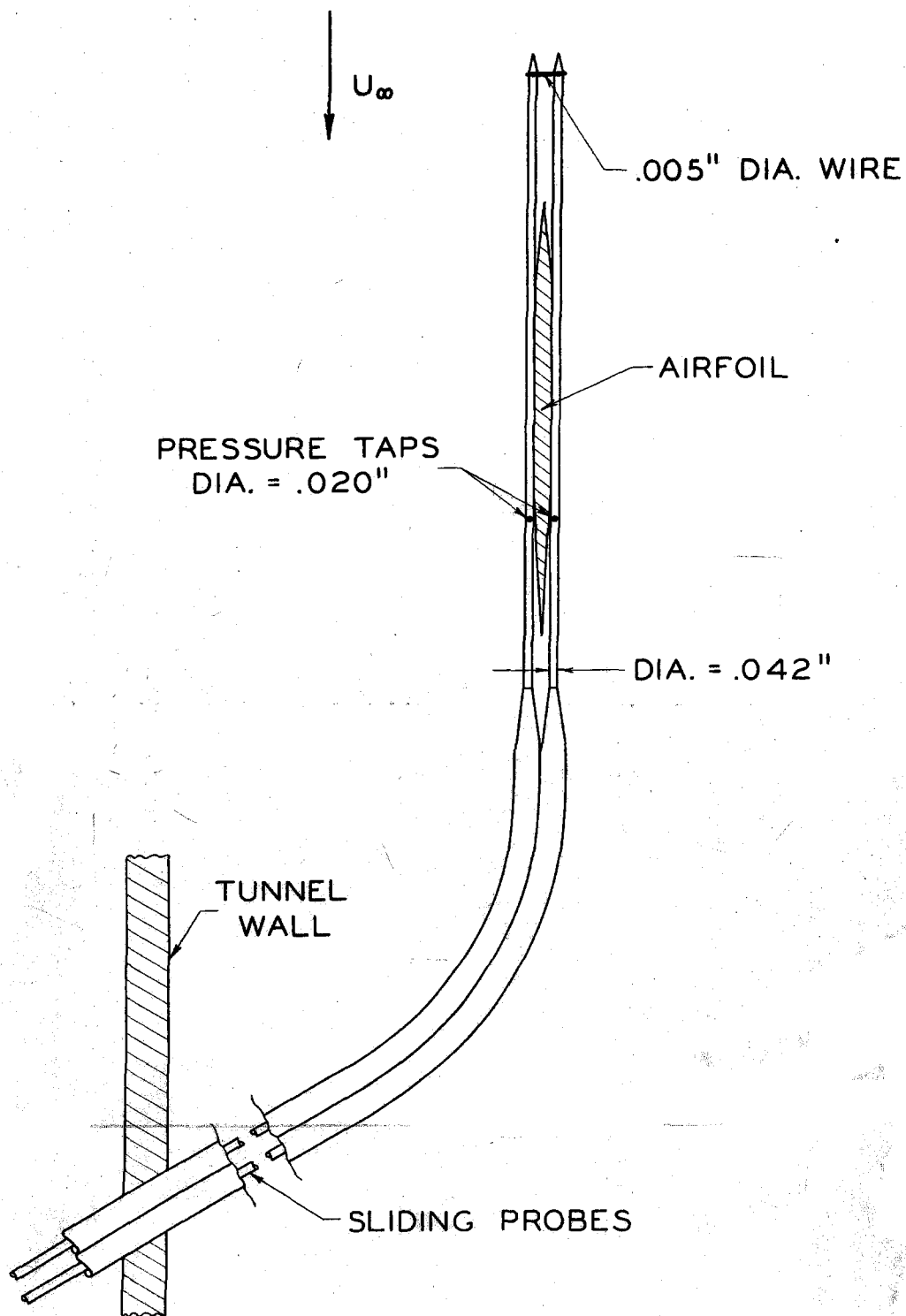
DOUBLE WEDGE

$C = 2''$

$t/c = .104$

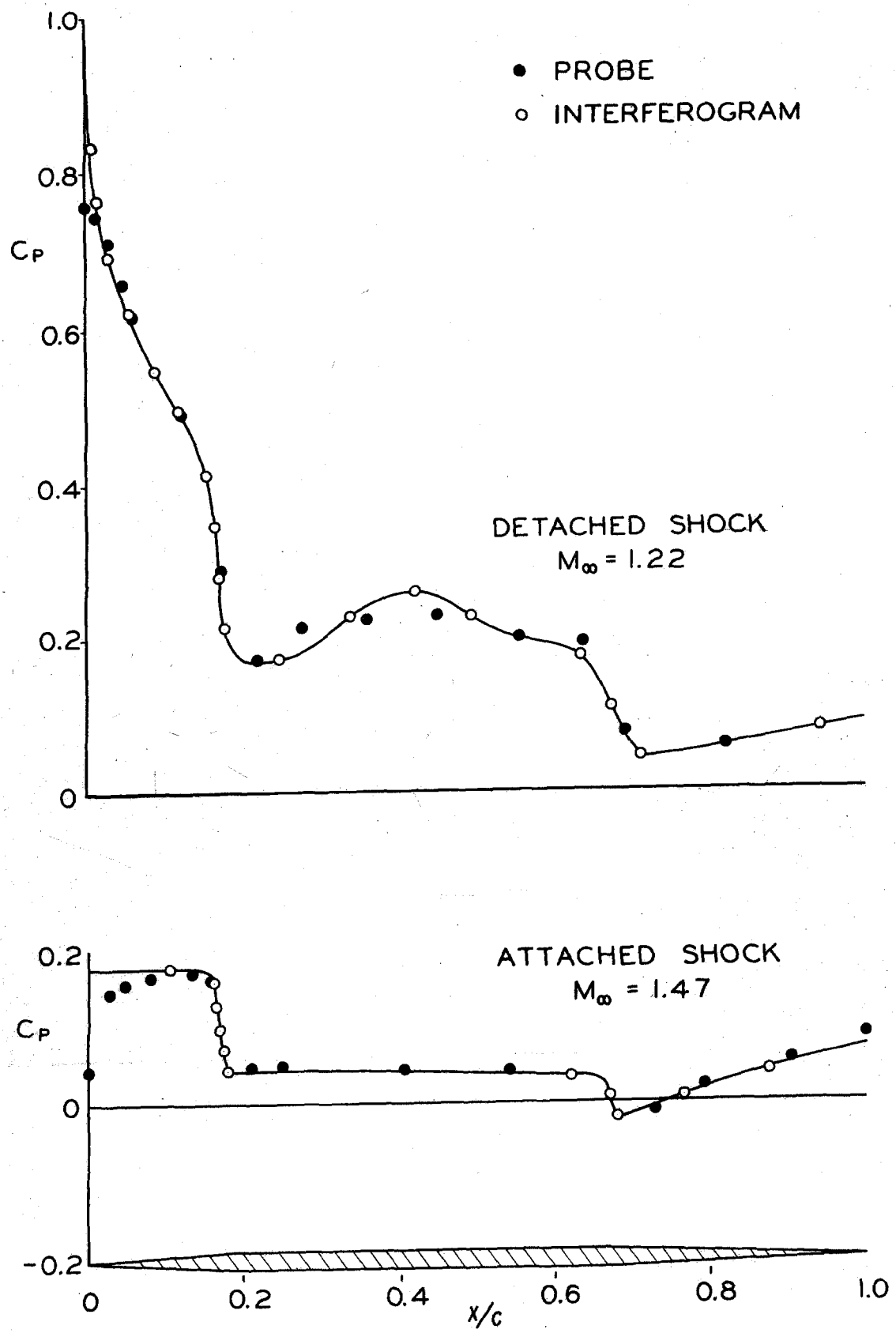
GEOMETRY OF AIRFOILS TESTED

FIG. 1



SCHEMATIC DRAWING OF SURFACE PRESSURE PROBE

FIG. 2



PROBE AND INTERFEROMETER SURFACE PRESSURES

FIG. 3

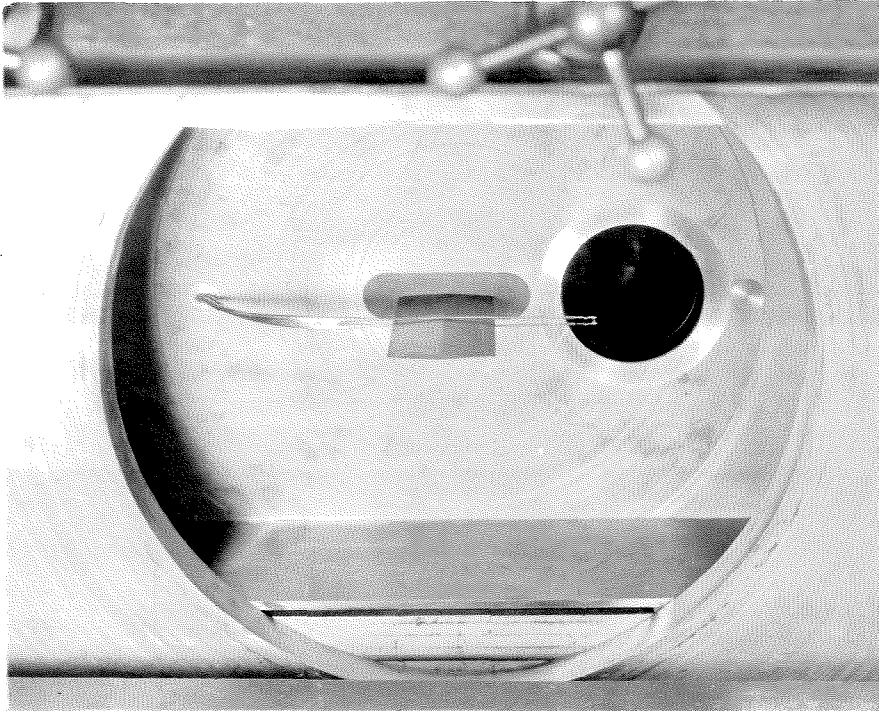
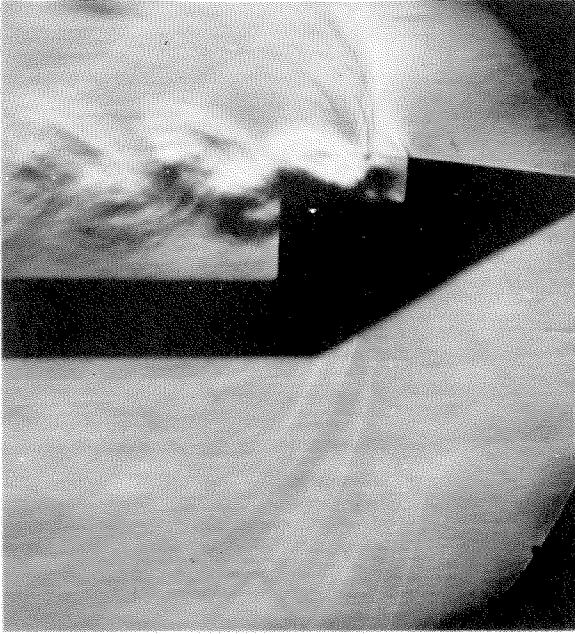
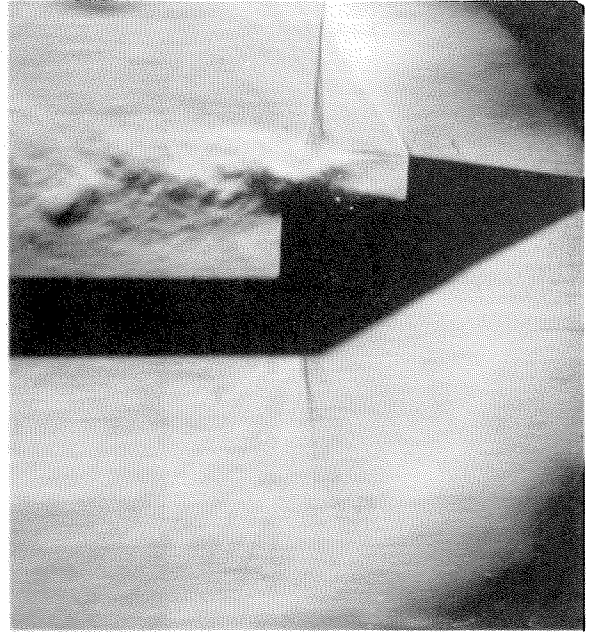


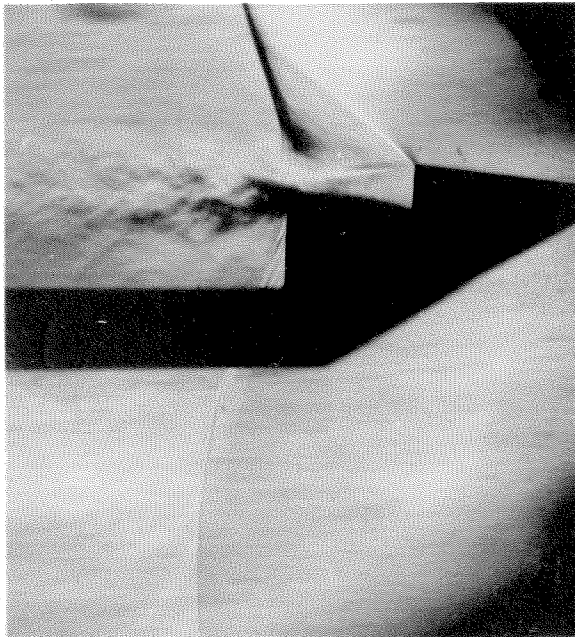
Fig. 4 - Surface Pressure Probe and Double Wedge
Installed in Wind Tunnel



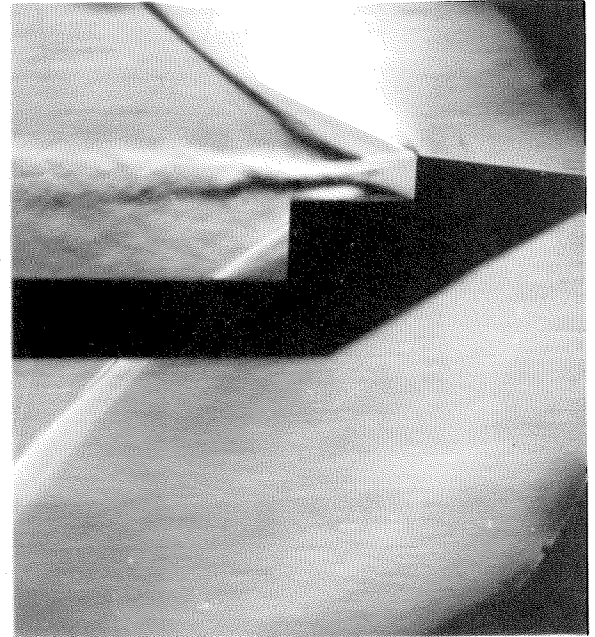
$M_\infty = .773 \quad \alpha = 0^\circ$



$M_\infty = .812 \quad \alpha = 0^\circ$

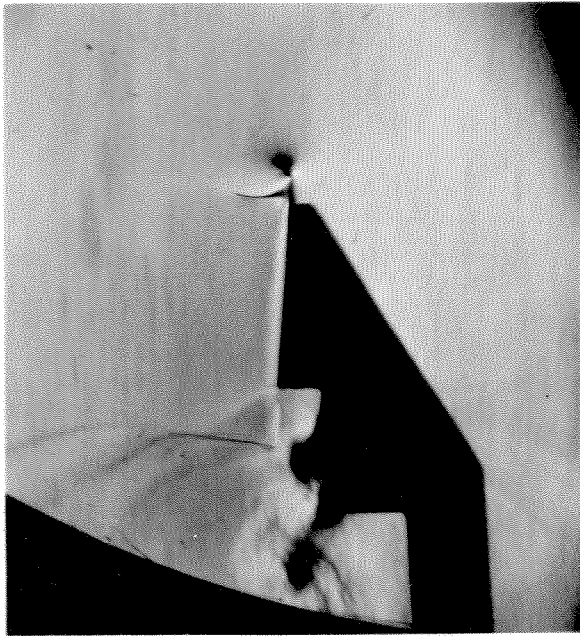


$M_\infty = .838 \quad \alpha = 0^\circ$

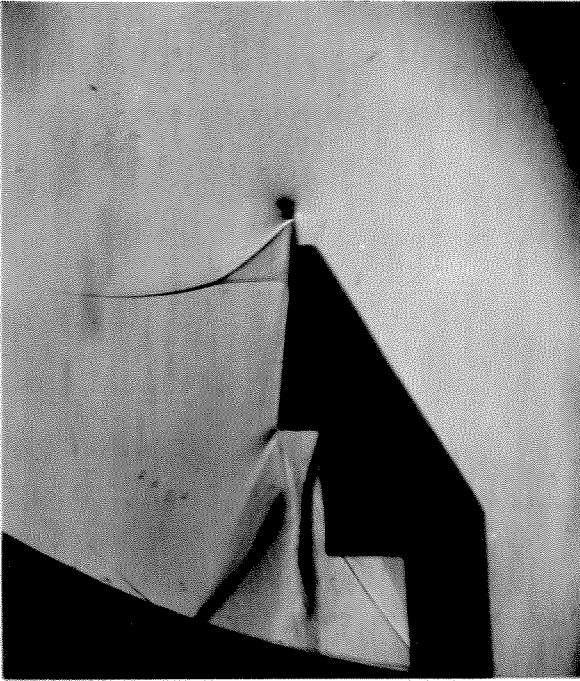


$M_\infty = .852 \quad \alpha = 0^\circ$

Fig. 5 - Flow Over a Truncated Wedge at Zero Angle of Attack $\delta = 5.97^\circ$

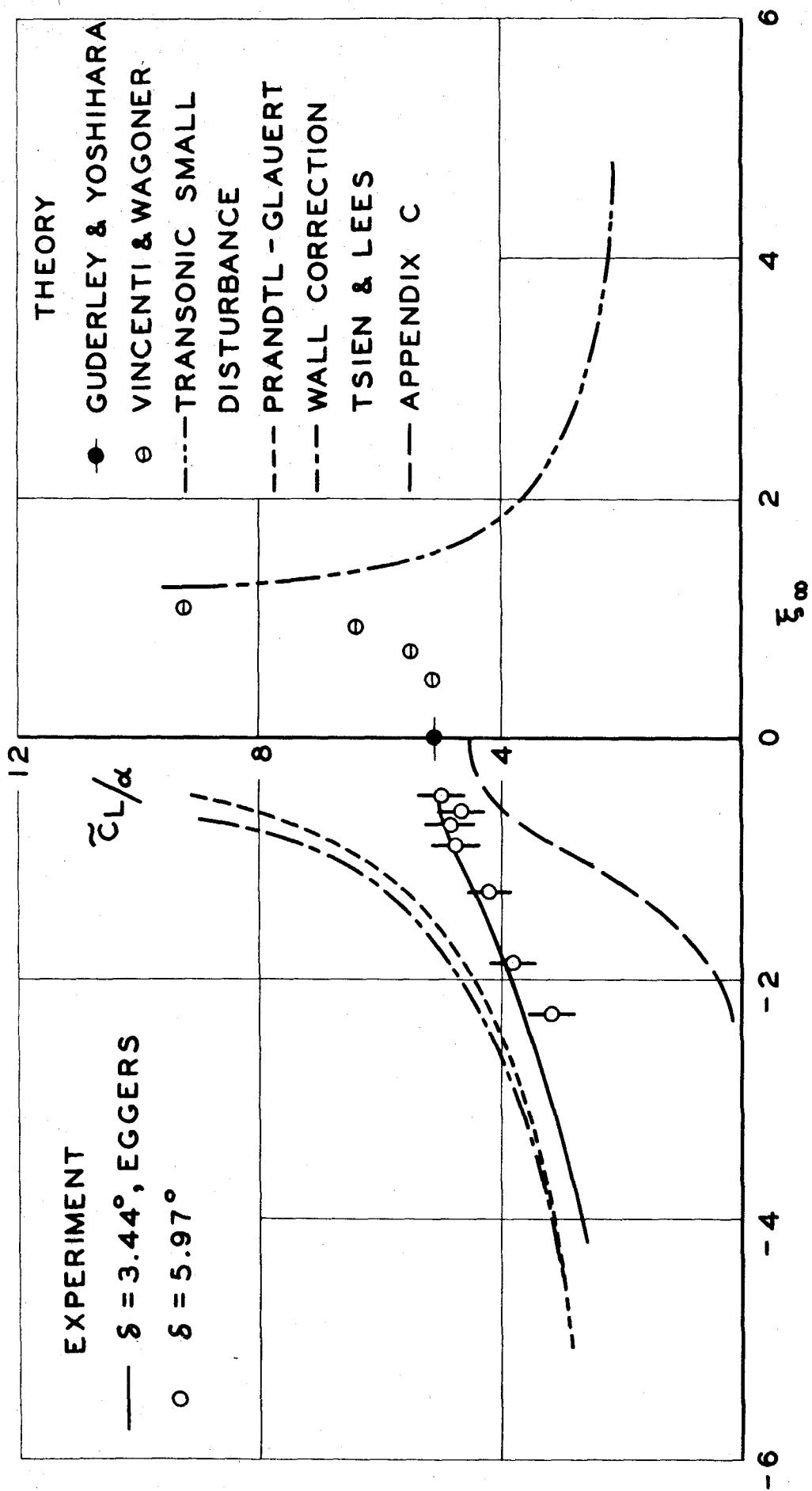


$$M_\infty = .785 \quad \alpha = 2^\circ$$



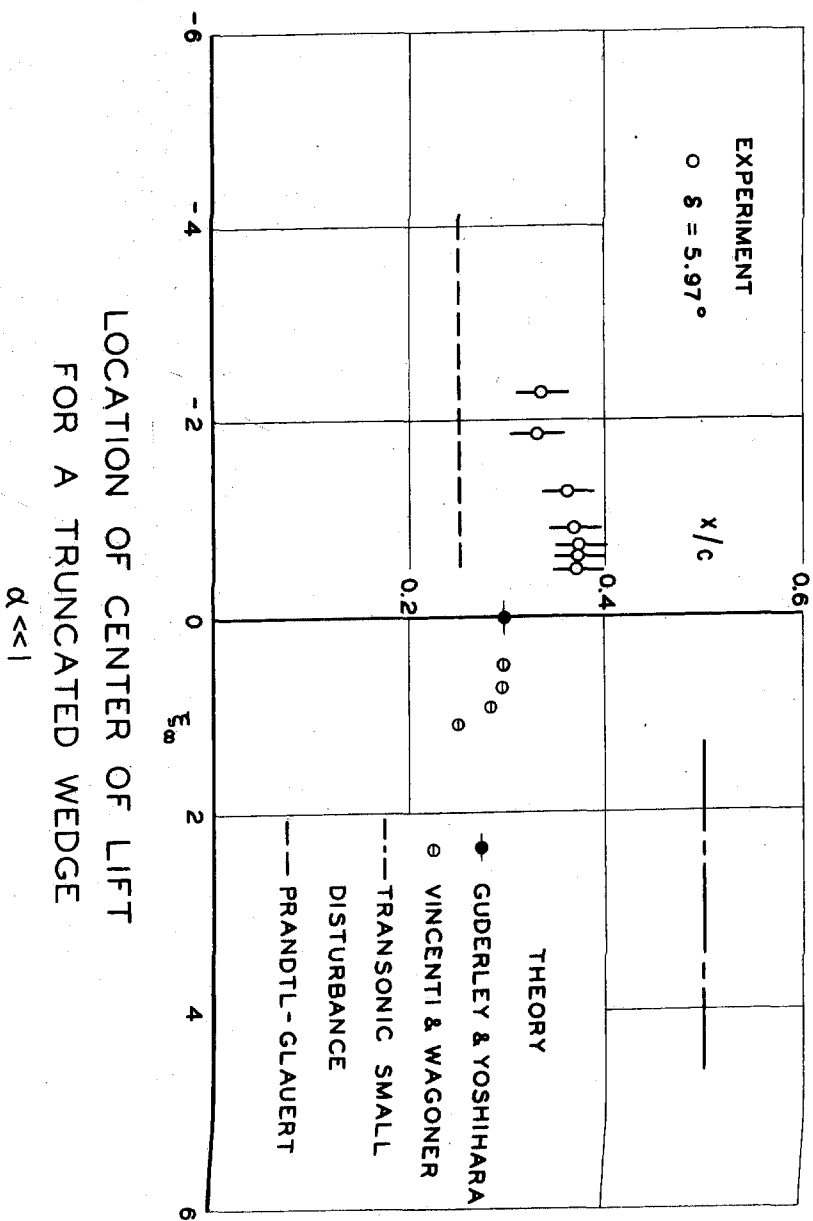
$$M_\infty = .863 \quad \alpha = 2^\circ$$

Fig. 6 - Flow Over a Lifting Truncated Wedge $\delta = 5.97^\circ$



LIFT OF A TRUNCATED WEDGE

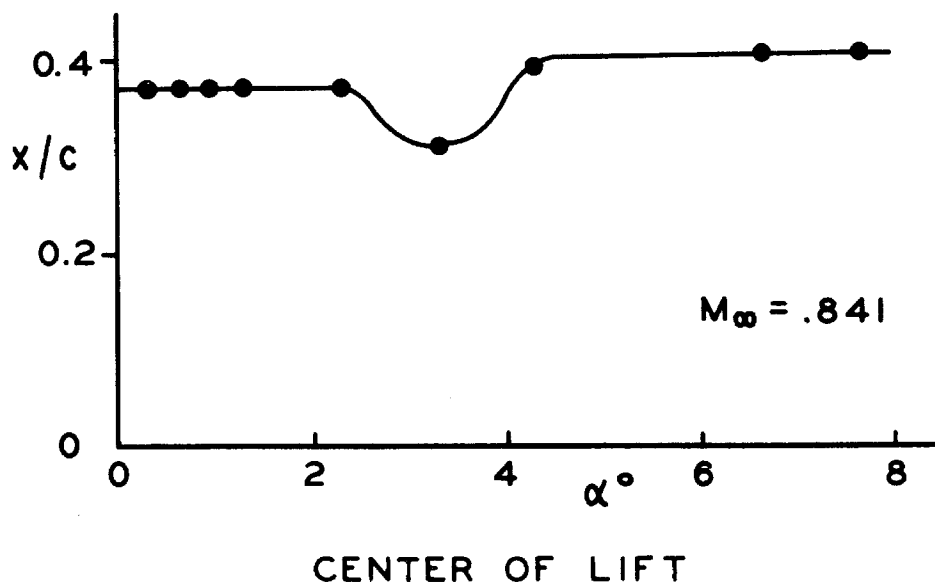
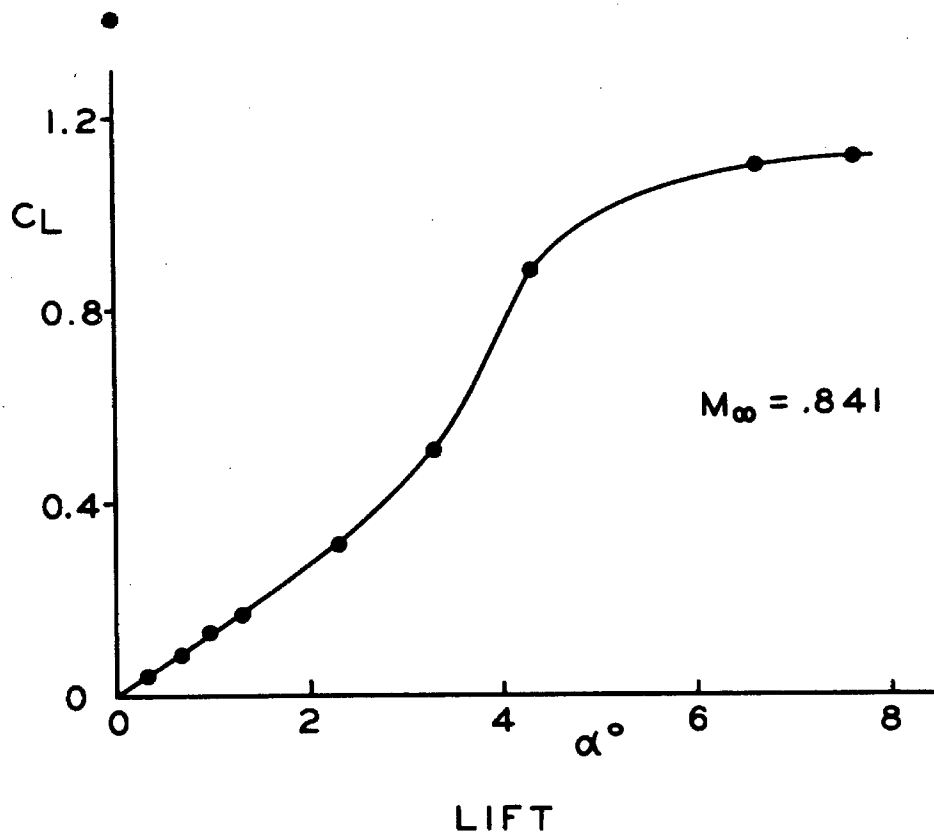
FIG. 7



LOCATION OF CENTER OF LIFT
 FOR A TRUNCATED WEDGE

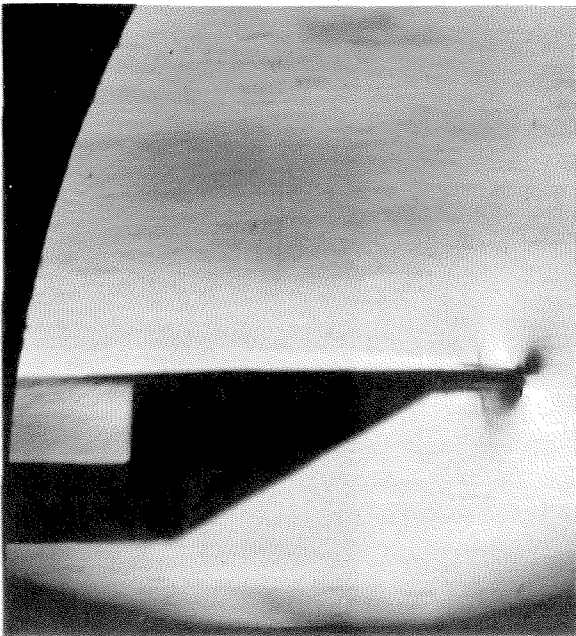
$$\alpha \ll 1$$

FIG. 8

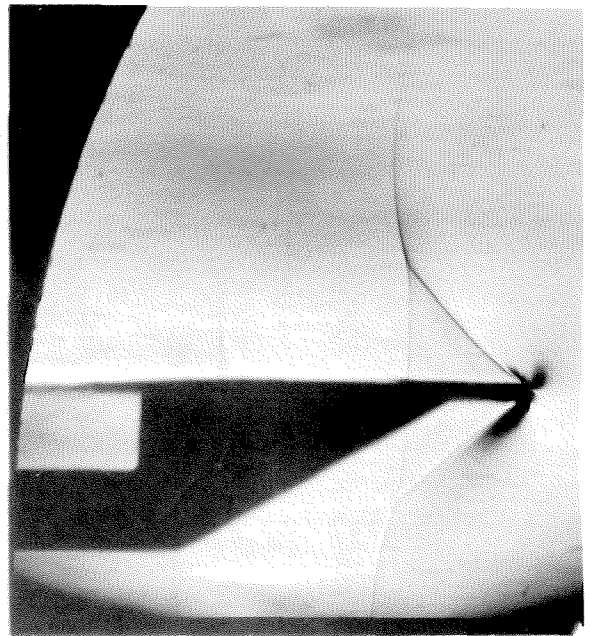


TRUNCATED WEDGE AT
LARGE ANGLES OF ATTACK

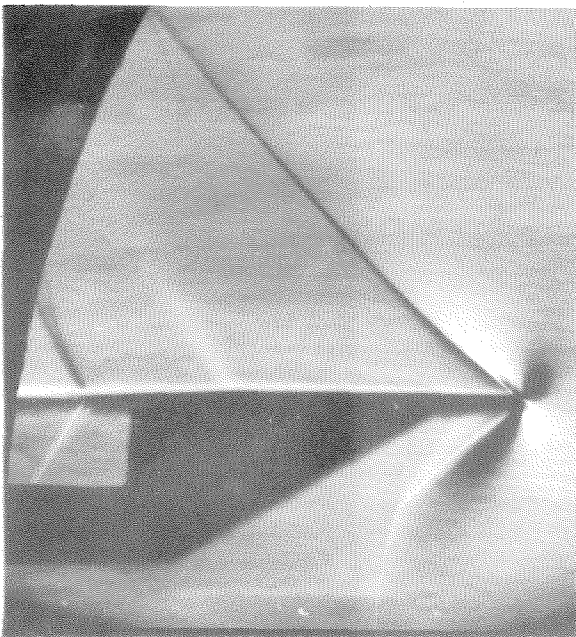
FIG. 9



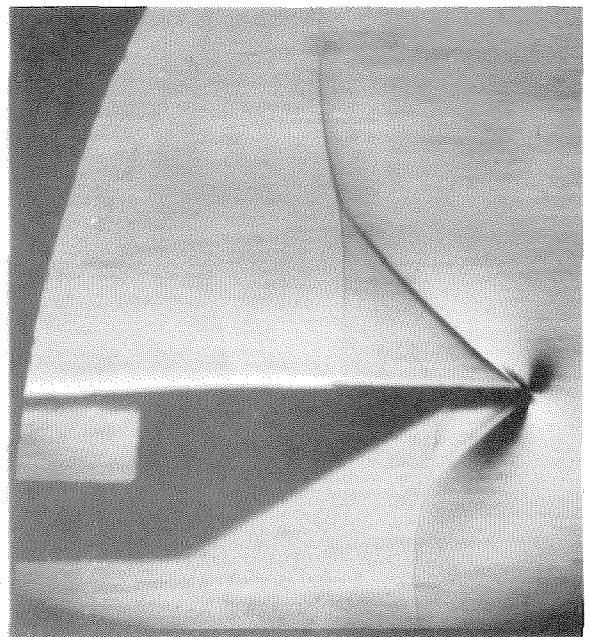
$M_\infty = .803 \quad \alpha = 0^\circ$



$M_\infty = .897 \quad \alpha = 0^\circ$

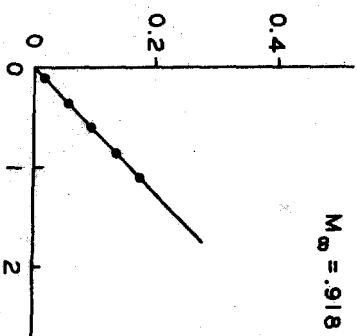
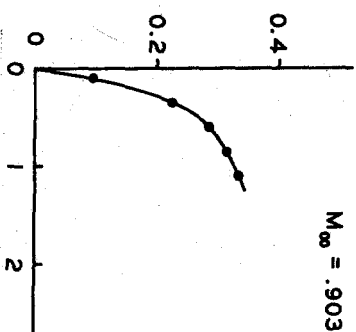
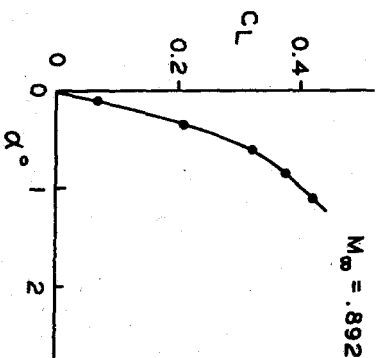
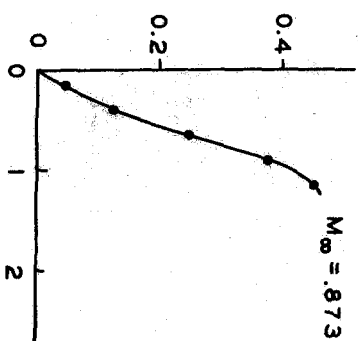
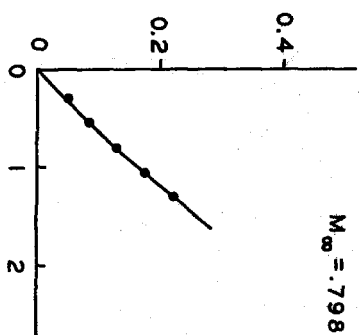
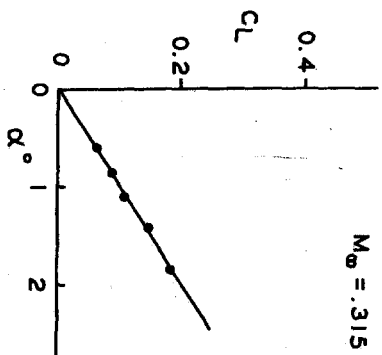


$M_\infty = .915 \quad \alpha = 0^\circ$



$M_\infty = .897 \quad \alpha = .2^\circ$

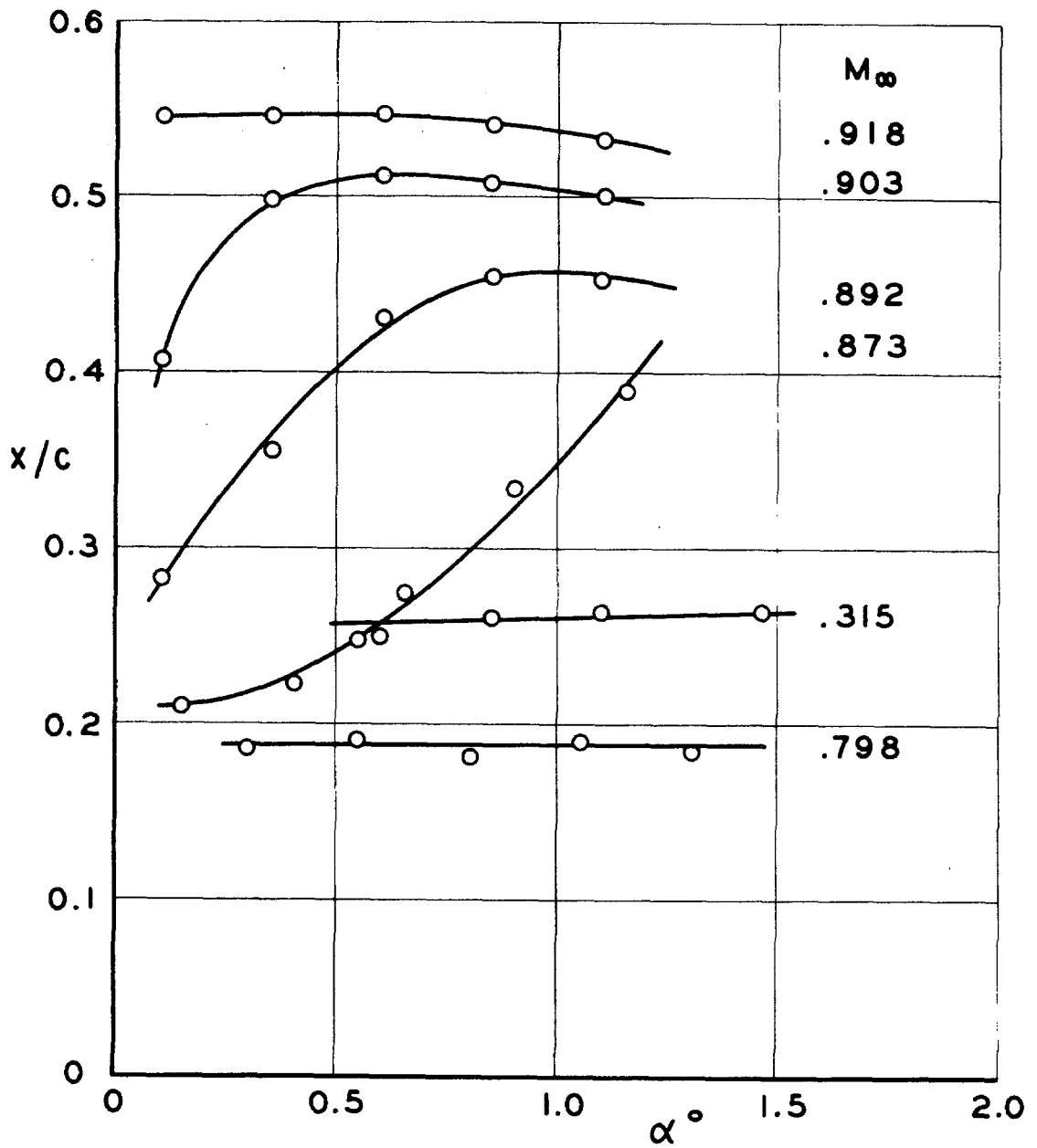
Fig. 10 - Flow Over Round Nose Airfoil $t/c = 0.033$



LIFT COEFFICIENT OF ROUND NOSE AIRFOIL

$t/c = .033$

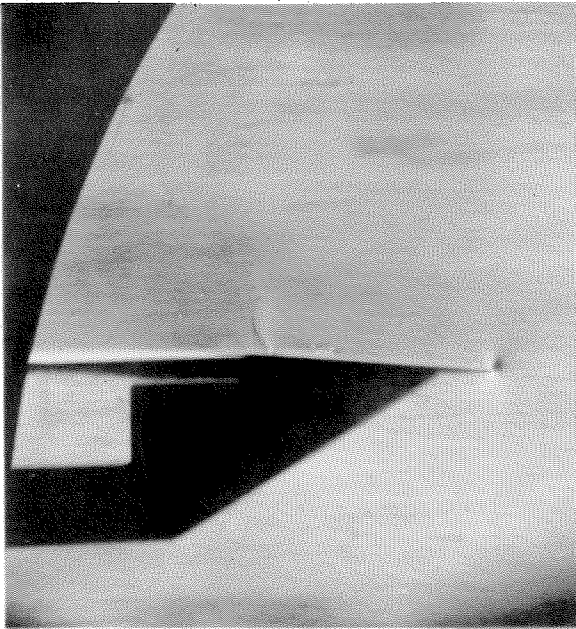
FIG. 11



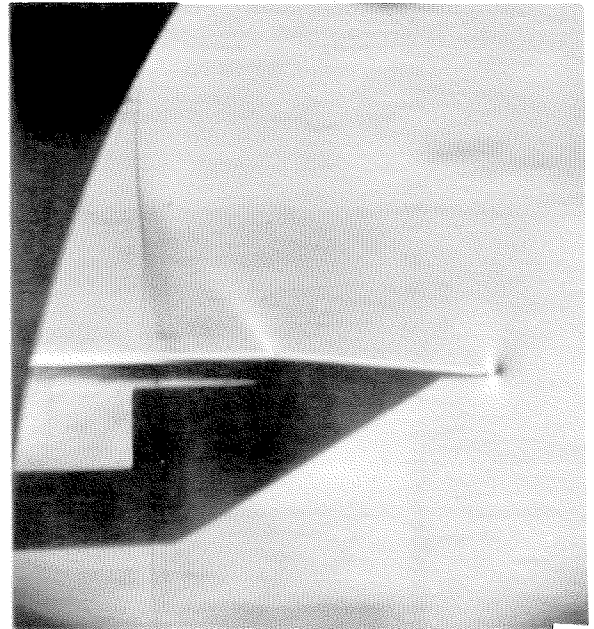
LOCATION OF CENTER OF LIFT
FOR ROUND NOSE AIRFOIL

$$t/c = .033$$

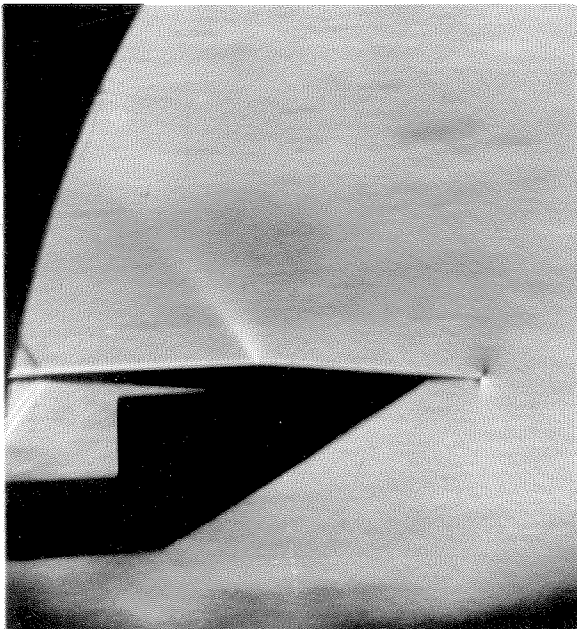
FIG. 12



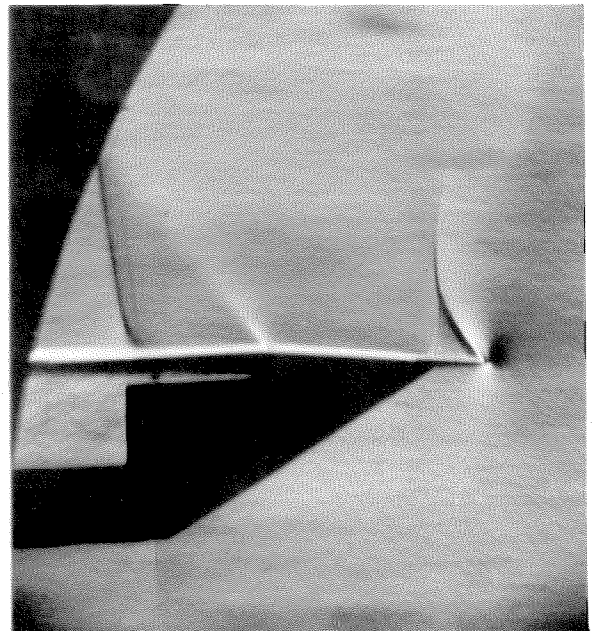
$M_\infty = .805 \quad \alpha = 0^\circ$



$M_\infty = .879 \quad \alpha = 0^\circ$

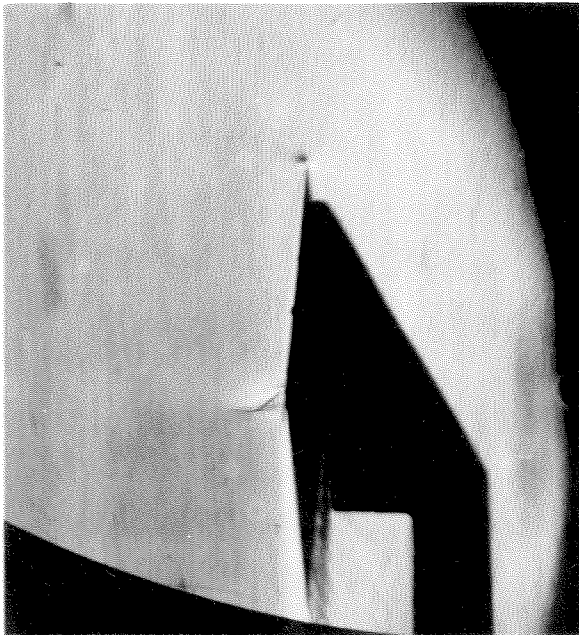


$M_\infty = .913 \quad \alpha = 0^\circ$

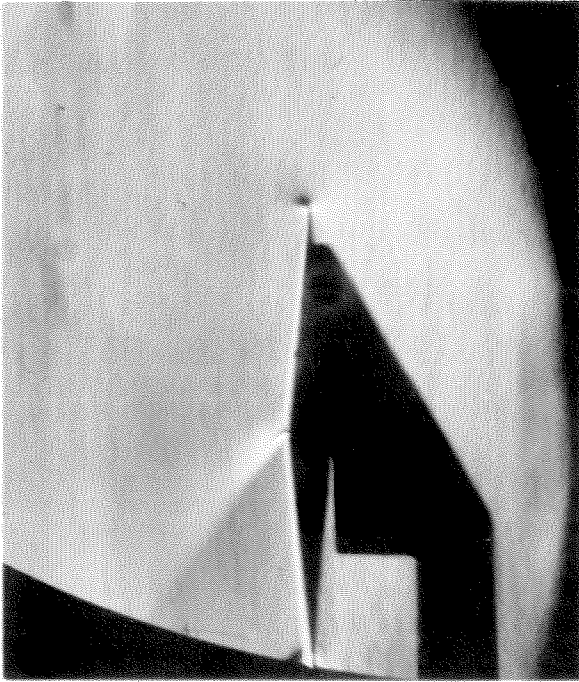


$M_\infty = .879 \quad \alpha = 1.5^\circ$

Fig. 13 - Flow Over a Double Wedge $t/c = 0.054$

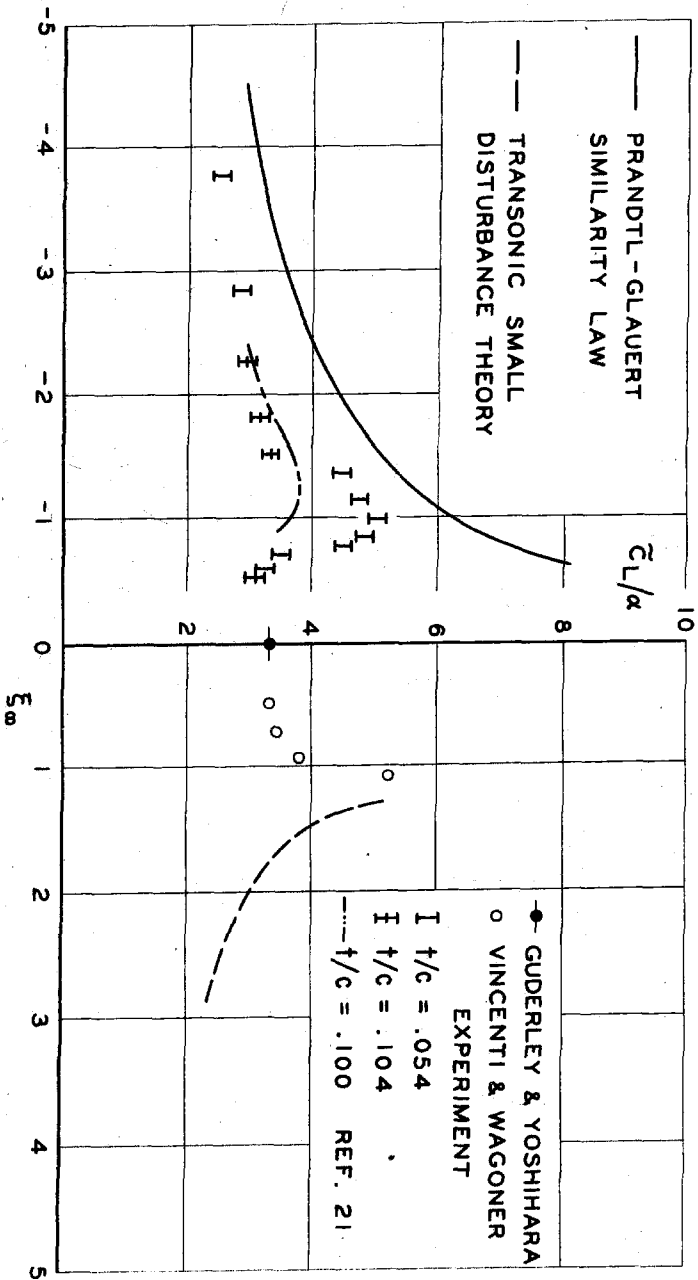


$M_\infty = .730$ $\alpha = 0^\circ$



$M_\infty = .878$ $\alpha = 0^\circ$

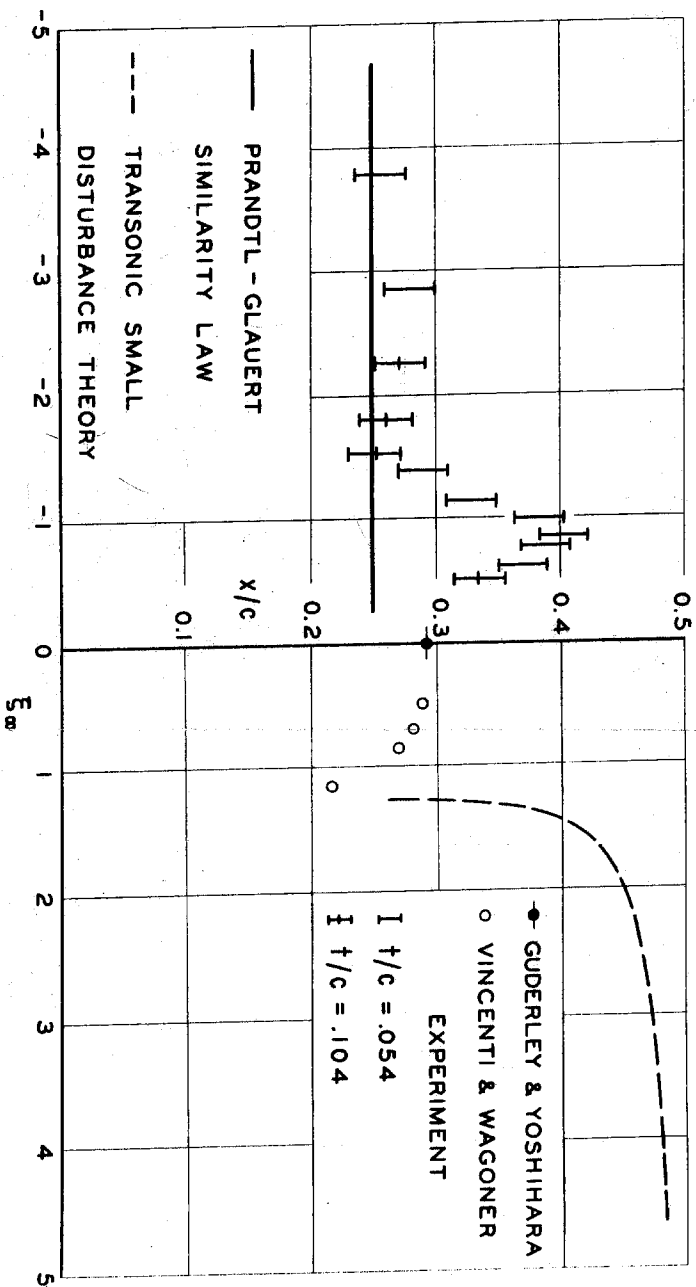
Fig. 14 - Flow Over a Double Wedge with Negligible Separation $t/c = 0.014$



LIFT CURVE SLOPE OF A DOUBLE WEDGE

$\alpha \ll 1$

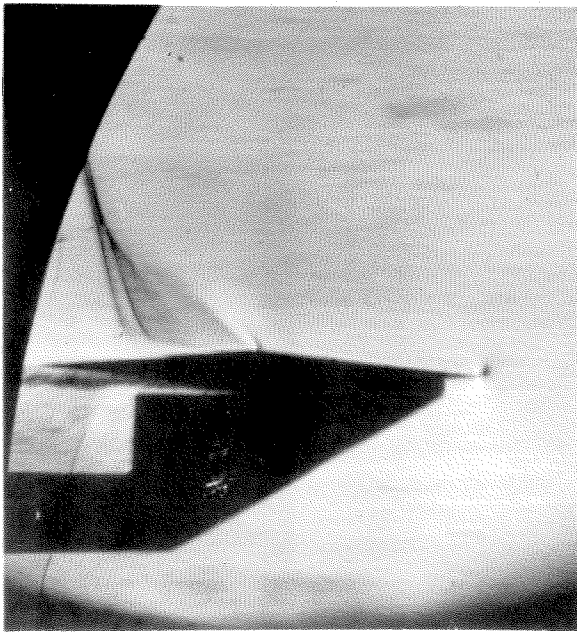
FIG. 15



CENTER OF LIFT FOR A DOUBLE WEDGE

$$\alpha \ll 1$$

FIG. 16



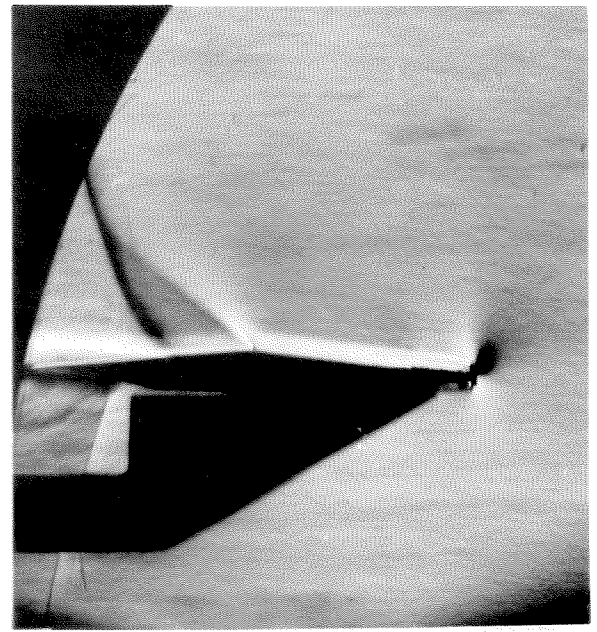
$M_{\infty} = 0.848$ $\alpha = 1^{\circ}$ No Rake



$M_{\infty} = 0.848$ $\alpha = 0^{\circ}$ Rake

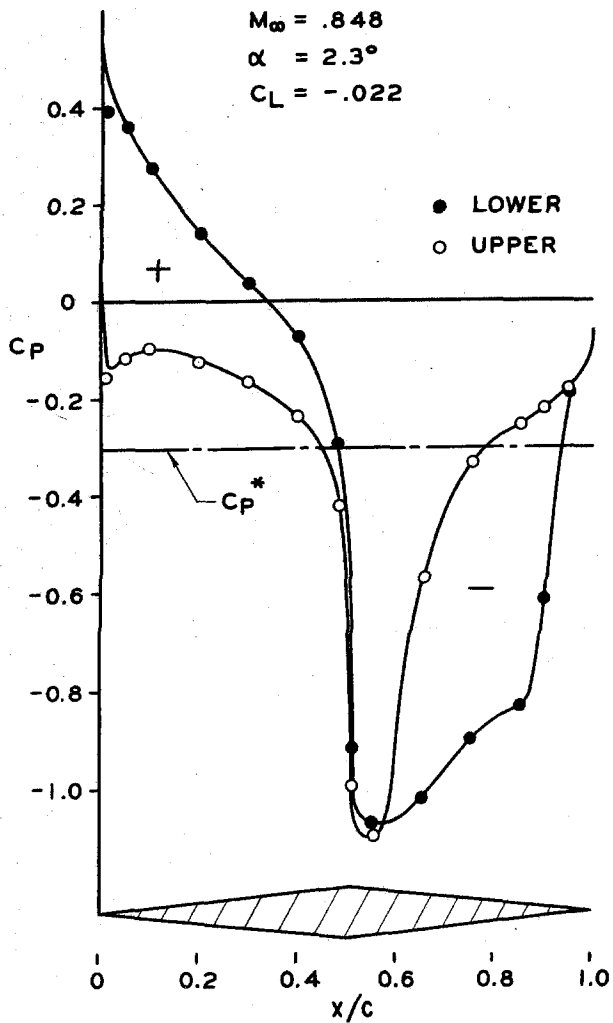


$M_{\infty} = 0.848$ $\alpha = 0^{\circ}$ No Rake



$M_{\infty} = 0.848$ $\alpha = 1^{\circ}$ Rake

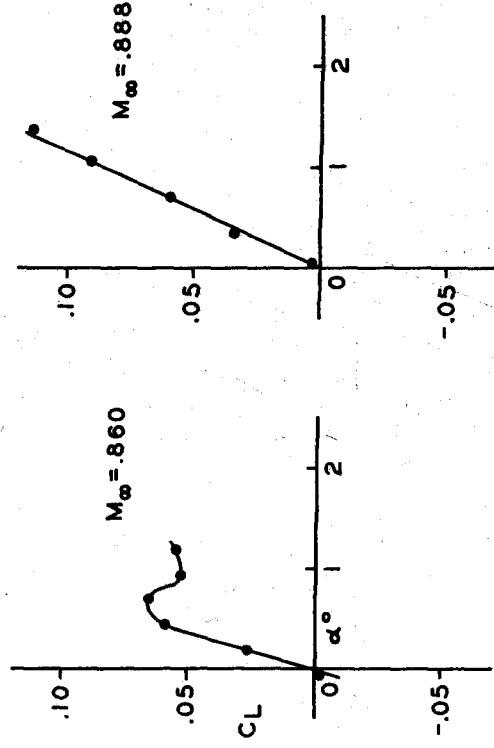
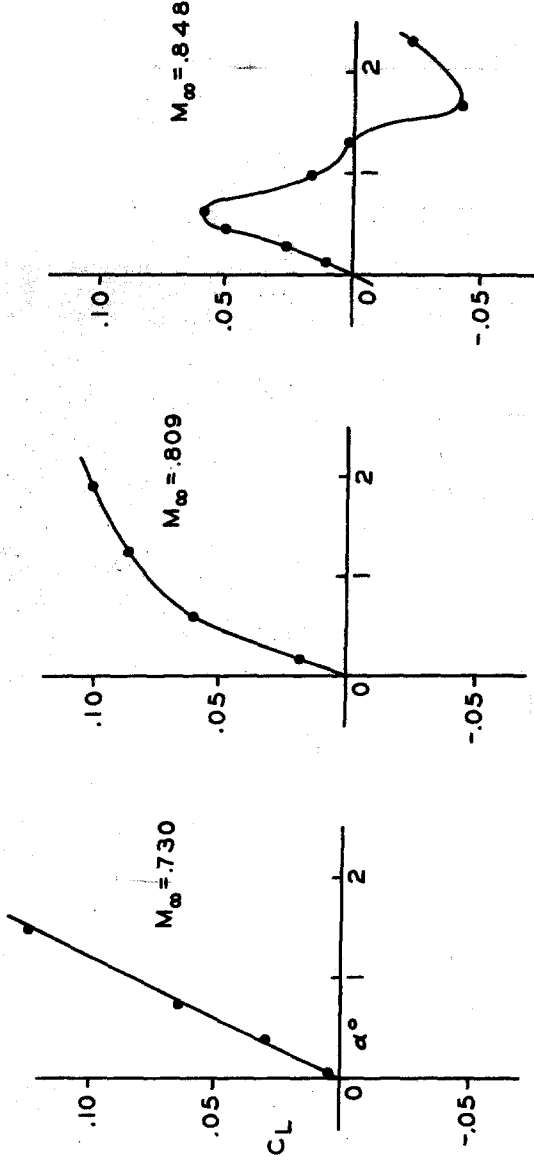
Fig. 17 - Separated Flow Over Rear Portion of a Double Wedge $t/c = 0.104$



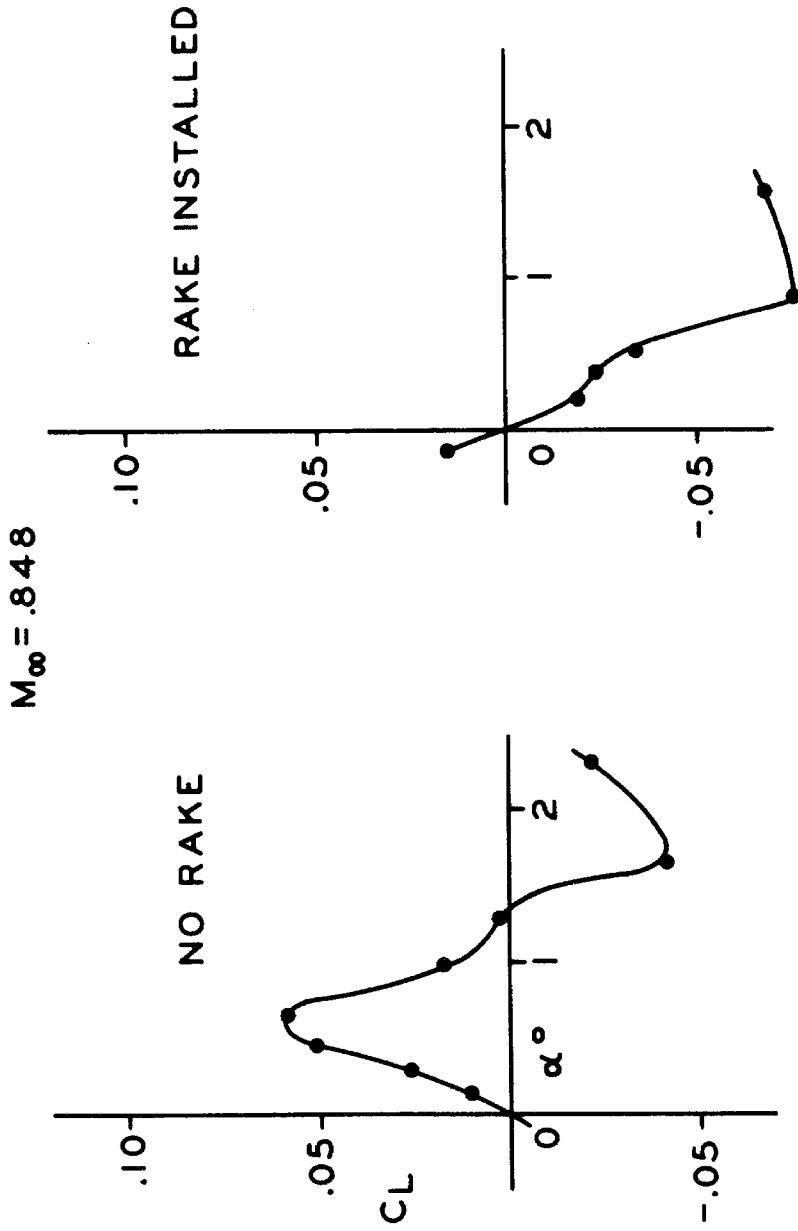
PRESSURE DISTRIBUTION ON A
 DOUBLE WEDGE WITH SEPARATION
 $t/c = .104$

FIG. 18

NO RAKE



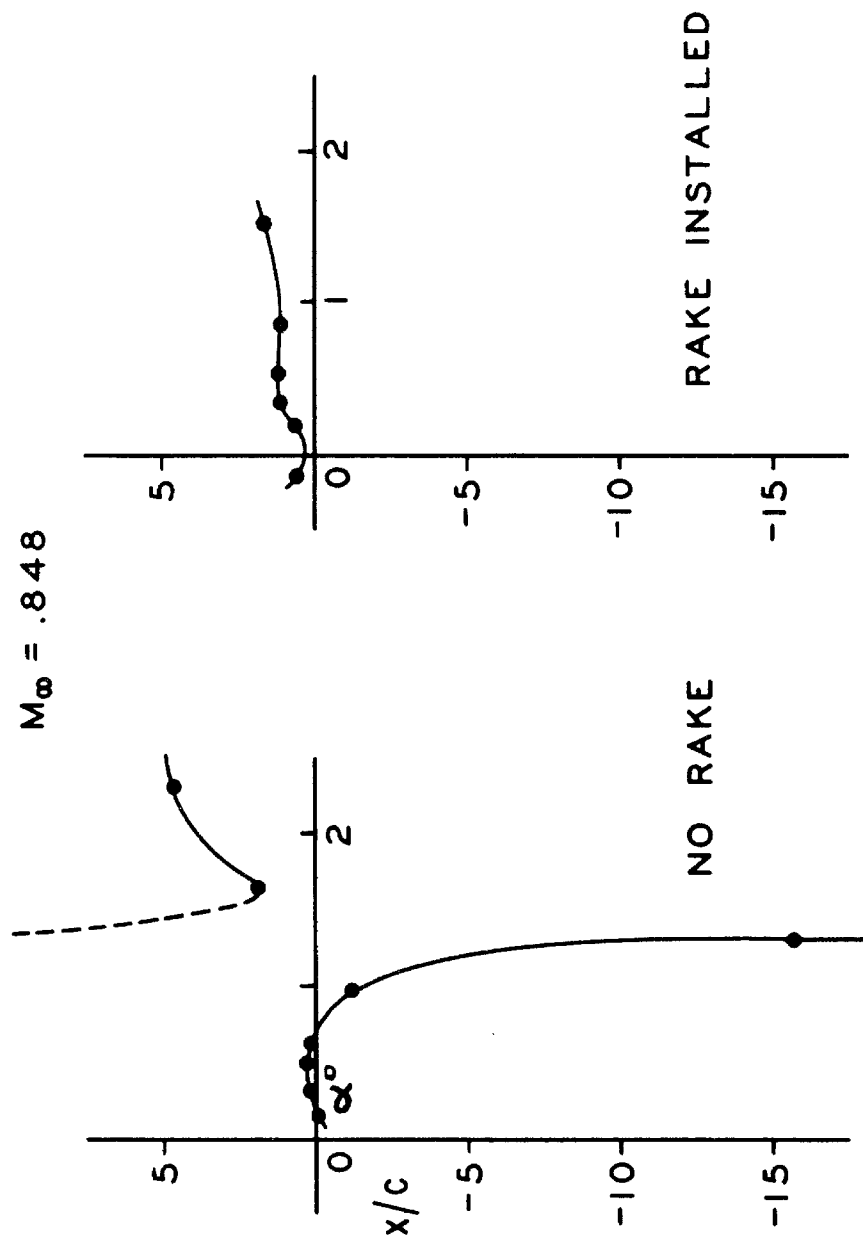
EFFECT OF SEPARATION ON LIFTING
DOUBLE WEDGE
 $t/c = .104$



EFFECT OF RAKE ON SEPARATION FOR
LIFTING DOUBLE WEDGE

$$t/c = .104$$

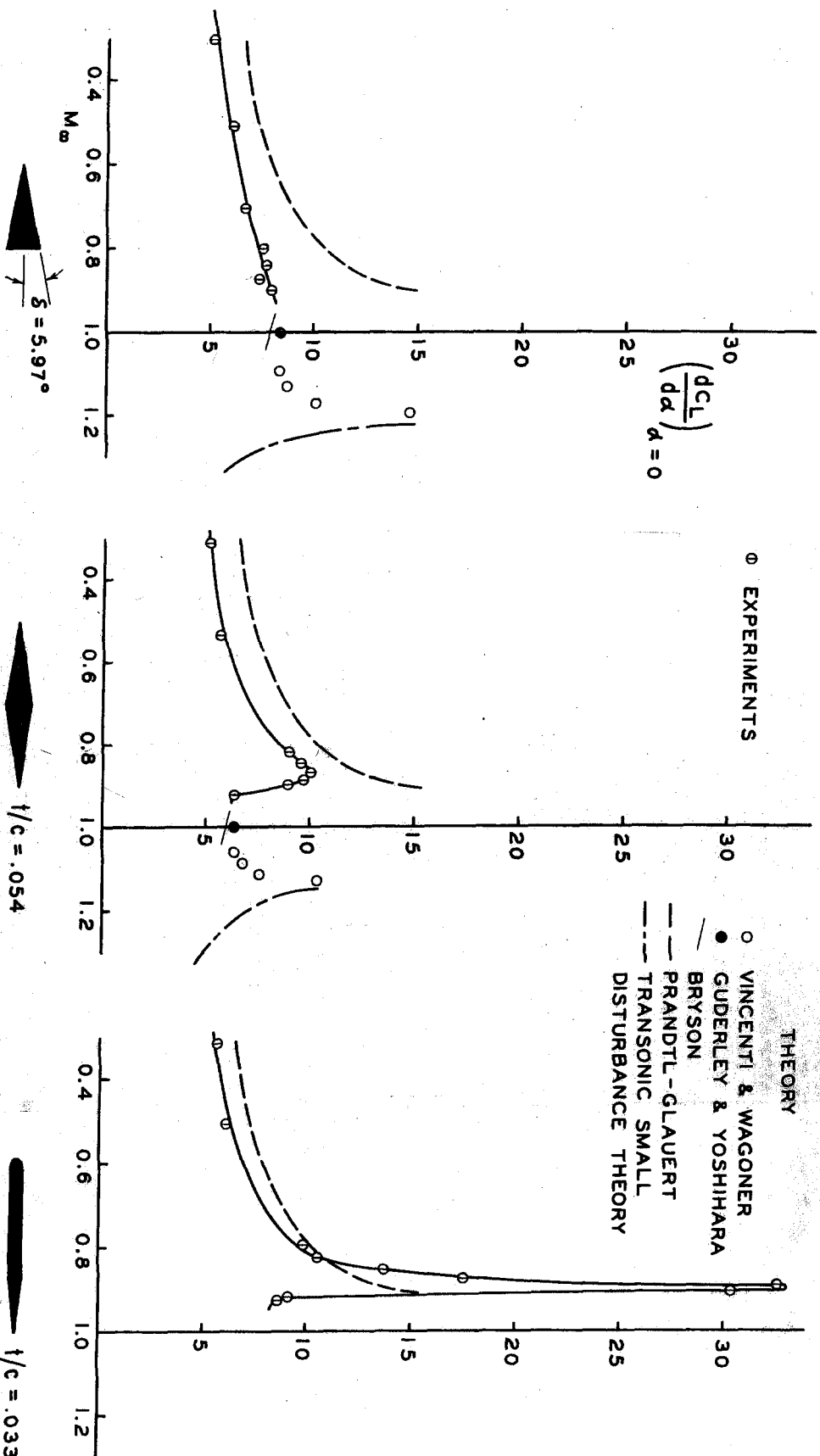
FIG. 20



CENTER OF LIFT FOR A
DOUBLE WEDGE WITH SEPARATION

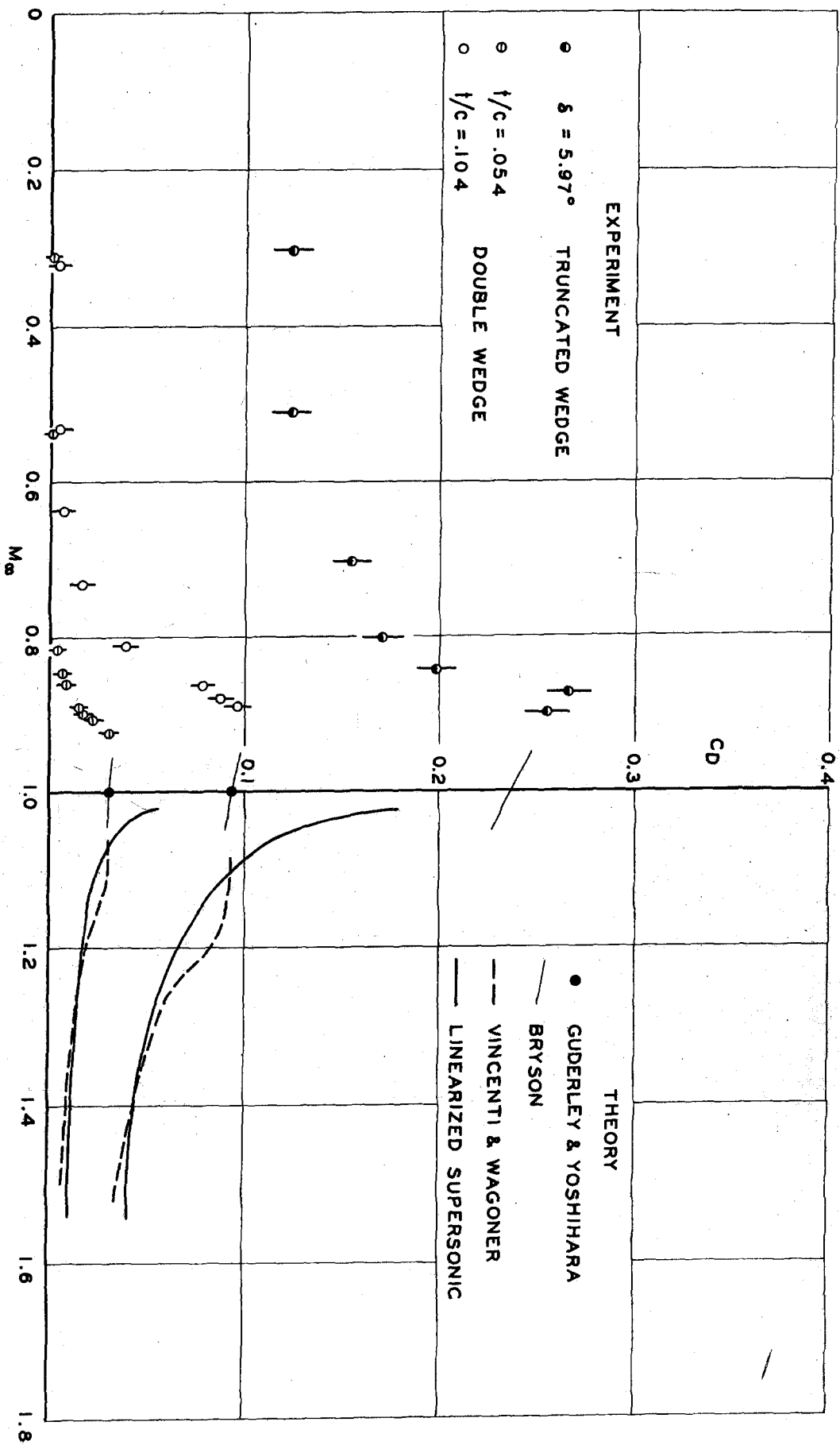
$$t/c = .104$$

FIG. 21



LIFT CURVE SLOPE FOR VARIOUS AIRFOIL SHAPES

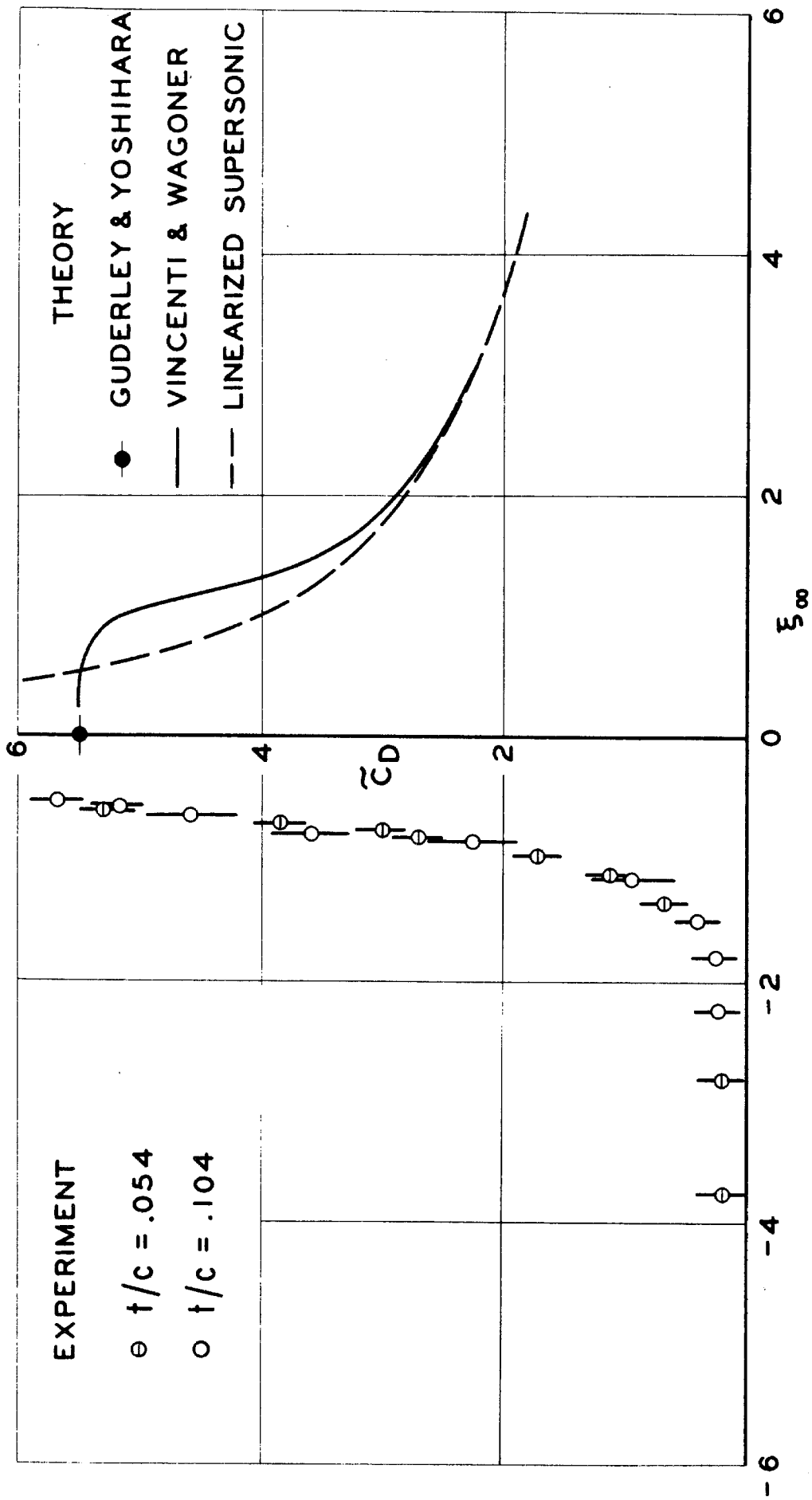
FIG. 22



DRAG COEFFICIENT OF WEDGES

$\alpha = 0$

FIG.23



DRAG COEFFICIENT OF A DOUBLE WEDGE

$$\alpha = 0$$

FIG. 24